Environ Monit Assess (2011) 180:345–369
DOI 10.1007/s10661-010-1792-x

Time-lapse resistivity investigation of salinity changes at an ex-promontory land: a case study of Carey Island, Selangor, Malaysia

Mohamad Faizal Tajul Baharuddin · Samsudin Taib · Roslan Hashim · Mohd Hazreek Zainal Abidin · Mohd Fakhrurrazi Ishak

Received: 15 April 2010 / Accepted: 9 November 2010 / Published online: 7 December 2010

Abstract Time-lapse resistivity measurements and groundwater geochemistry were used to study salinity effect on groundwater aquifer at the ex-promontory-land of Carey Island in Malaysia. Resistivity was measured by ABEM Terrameter SAS4000 and ES10-64 electrode selector. Relationship between earth resistivity and total dissolved solids (TDS) was derived, and with resistivity images, used to identify water types: fresh ($\rho_e > 6.5\ \Omega$ m), brackish ($3\ \Omega$ m $< \rho_e < 6.5\ \Omega$ m), or saline ($\rho_e < 3\ \Omega$ m). Long-term monitoring of the studied area's groundwater quality via measurements of its time-lapse resistivity showed salinity changes in the island's groundwater aquifers not conforming to seawater-freshwater hydraulic gradient. In some aquifers far from the coast, saline water was dominant, while in some others, freshwater 30 m thick showed groundwater potential. Land transformation is believed to have changed the island's hydrogeology, which receives saltwater pressure all the time, limiting freshwater recharge to the groundwater system. The time-lapse resistivity measurements showed active salinity changes at resistivity-image bottom moving up the image for two seasons' (wet and dry) conditions. The salinity changes are believed to have been caused by incremental tide passing through highly porous material in the active-salinity-change area. The study's results were used to plan a strategy for sustainable groundwater exploration of the island.

Keywords Salinity · Groundwater chemistry · Time-lapse resistivity · Ex-promontory land

M. F. Tajul Baharuddin (✉) · R. Hashim
Department of Civil Engineering, Faculty of Engineering, University of Malaya, 50603 Kuala Lumpur, Malaysia
e-mail: mdfaizal@uthm.edu.my

S. Taib
Department of Geology, Faculty of Science, University of Malaya, 50603 Kuala Lumpur, Malaysia

M. F. Tajul Baharuddin · M. H. Zainal Abidin
Department of Geotechnical and Transportation Engineering, Faculty of Civil and Environmental Engineering, Tun Hussein Onn University, 86400 Batu Pahat, Johor, Malaysia

M. F. Ishak
Faculty of Civil and Earth Resources Engineering, University of Malaysia Pahang, 25300 Kuantan, Pahang, Malaysia

Introduction

Salinity of groundwater aquifers, especially at coastal regions, changes naturally or through human activity. A major cause, sometimes affecting freshwater quality, is seawater intrusion. Excessive withdrawing of groundwater, and significant

decrease in recharge, too, contribute (Pujari and Soni 2008). Aquifer-salinity changes naturally when low-density fresh groundwater interacts with high-density saltwater. The best geophysical method, particularly in salinity mapping, is geo-electrical method (Loke 2010a). Researchers demarcating coast hydrogeology have been using geo-electrical method to map salinity ever since development of the interpretation technique by Loke and Barker (1996). Electrical resistivity method is unique as it detects increased aquifer conductivity via increased pore-water conductivity (Abdul Nassir et al. 2000). Benkabbour et al. (2004) used geophysical method to characterize saltwater intrusion in the Plioquaternary consolidated coastal aquifer of the Mamora Plains, Morocco. Di Sipio et al. (2006) used geo-electrical method and geochemistry data to get better salinity profile of the groundwater system in Venice estuaries. Awni (2006) used 2-D geo-electrical method to detect subsurface freshwater and saline water at the alluvial shoreline of the Dead Sea, Jordan. Sherif et al. (2006) integrated geo-electrical method with hydro-geochemical method to delineate saltwater intrusion at Wadi Ham, UAE. In Lagos, Nigeria, Adepelumi et al. (2009) used vertical-electrical-sounding survey to delineate Lekki Peninsula freshwater–aquifer saltwater intrusion.

The studies detected and mapped salinity at regions of spatial variations. Salinity changes are dynamic, happening every day in groundwater systems, especially at open-sea coastal, and estuarine, regions. Major factors relating to time

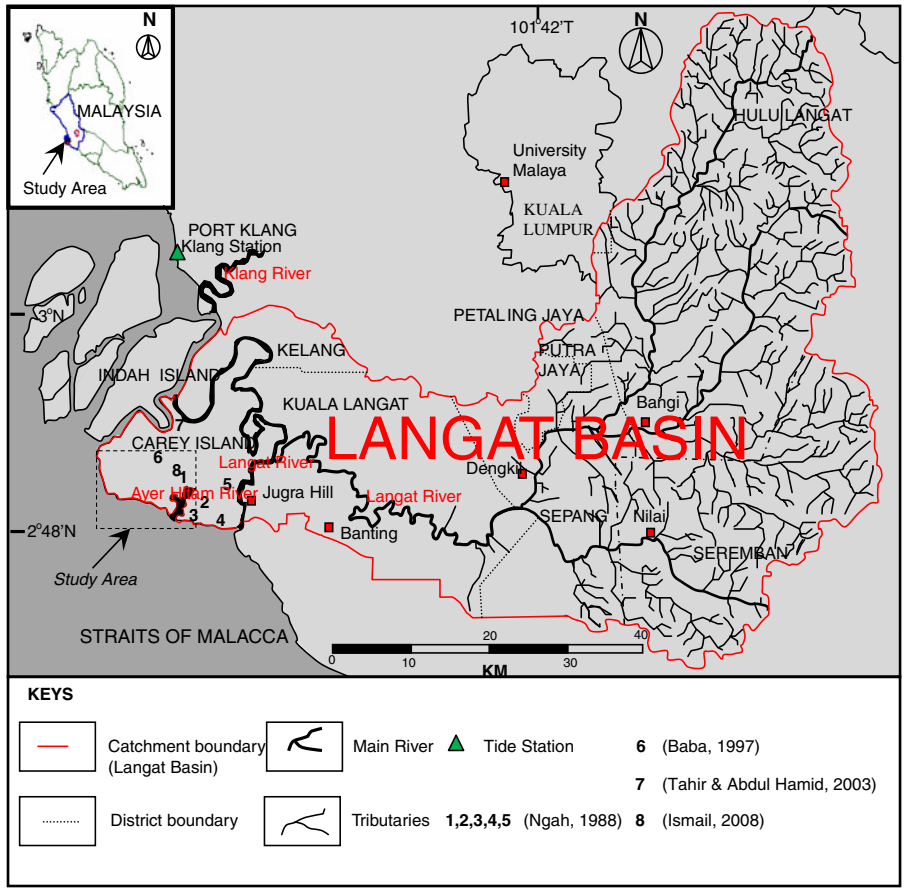

Fig. 1 Carey Island situated at downstream of Langat Basin. Note non-coverage by other works, of the majority of the area studied in this work

Note: (Names of Villages: 1&7=Sg. Judah; 2=Sg. Rambai; 3=Kenanga; 4=Kepau Laut; 5=Sg. Bumbun; 6=West Estate)

and space are tide, season, and seawater density. Geo-electric imaging surveys of space have been done, and can be done for time (Loke 2010a). Image analysis, from spatially distributed resistances at specific time intervals, is through time-lapse electrical-resistivity tomography (TLERT). TLERT's various applications have attracted many researchers: Barker and Moore (1998) for physical-model tests of groundwater flow and contamination; Kemna et al. (2002), Cassiani et al. (2006), and Oldenborger et al. (2007) for tracer-test study of aquifers; Olofsson and Lundmark (2009) for impact monitoring of roadside-soil de-icing-salt in saltwater investigation; and Ogilvy et al. (2009) for study of near-coast saltwater intrusion; in each, TLERT images relate change in salinity to transport of solutes.

TLERT is capable of minimal-invasion-monitoring of hydraulic processes in porous media by capturing temporal conductivity variations (Ogilvy et al. 2009). TLERT measurements fill, less expensively, gaps in data on space between sets of boreholes (Maillet et al. 2005). Acquisition of TLERT-image resistance data requires good electrical grounding during TLERT monitoring. Soil electrical conductivity is influenced by the complex interaction among soil's physical properties, water content, salinity, and ground temperature, all possibly influencing electrical grounding (Olofsson and Lundmark 2009). Poor electrical grounding disables data acquisition, resulting in incomplete resistivity data. Good electrical grounding takes time to prepare, but without it, image quality is affected, and the rate of change that can be captured with TLERT monitoring becomes limited. Discussed here are resistivity-acquisition techniques where poor electrical grounding is improved.

This work's concern is salinity changes to freshwater at Carey Island in the state of Selangor, Malaysia (Fig. 1). Carey Island, near Indah Island, is Malaysia's biggest trading port. Not only is it located in Malaysia's most advanced industrial and trading state (Selangor), it is also near Malaysia's administration centers of Putrajaya and Kuala Lumpur (capital city of Malaysia). Its infrastructure has grown rapidly, with highways mobilizing trade between it and South Peninsular Malaysia. Its population is expected to increase significantly when its entire infrastructure had been completed.

Selangor was predicted to be 1 million m^3 of water short daily in 2007 (Tahir and Abdul Hamid 2003). At Carey Island, the shortage was regular, so people harvested rain. Government agencies such as the Department of Mineral and Geo-

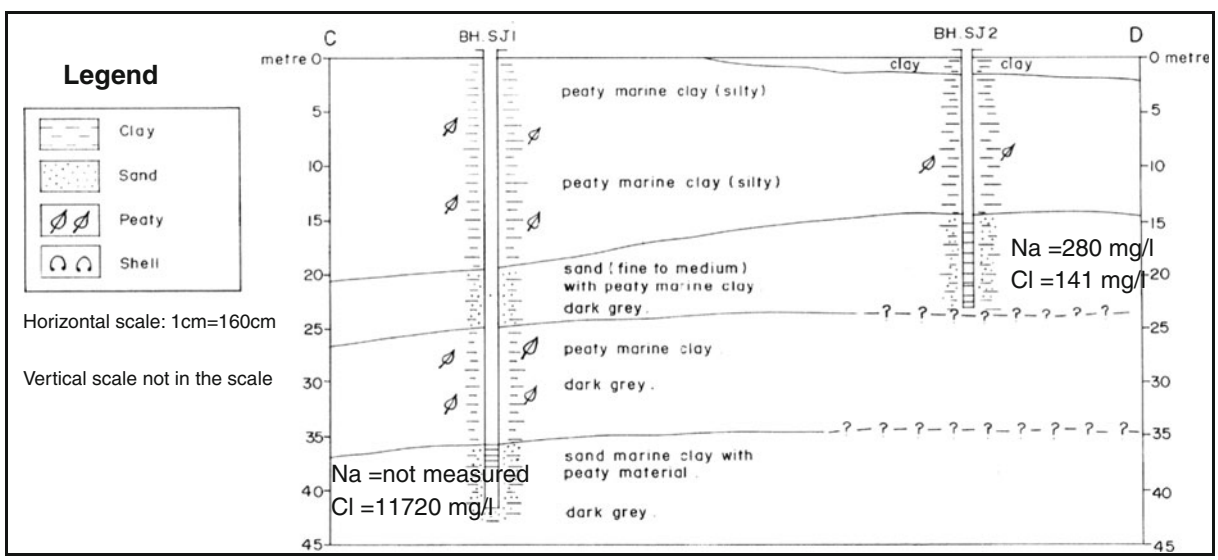

Fig. 2 Sg. Judah Village subsurface profile and geochemistry data at semi-confined aquifer (Ngah 1988)

Science were asked to determine the island's water-supply potential. On the district council's request, Ngah (1988) investigated groundwater at five aboriginal villages to determine shallow-aquifer potential (Fig. 1). Sg. Judah study revealed freshwater in aquifers less than 25 m deep. Thicknesses of semi-confined aquifers ranged between 5 and 7 m (Fig. 2). Some shallow semi-confined aquifers there especially at borehole SJ3 400 m south of borehole SJ2 was identified as having brackish water, chloride concentration 620 mg/l (Fig. 3). Aquifers more than 35 m deep were identified as not having promising groundwater potential because saline and brackish waters were more dominant. Tahir and Abdul Hamid continued investigations in 2003, as requested by the Malaysian Government and provisioned in the Eighth Malaysia Plan (2000–2005) for northern region. They revealed brackish-water domination, chloride concentration >250 mg/l, still, in groundwater 95 m deep. In 2008, Ismail furthered the study, encountering screen level at depths between 175 and 180 m; no potential for groundwater extraction (the groundwater was dominated by brackish water, conductivity value >2,000 μS/cm). Preceding effort was to understand the area's hydrogeology so its groundwater-exploration could be strategized. Efforts by relevant government agencies to identify the best strategy have been unsuccessful.

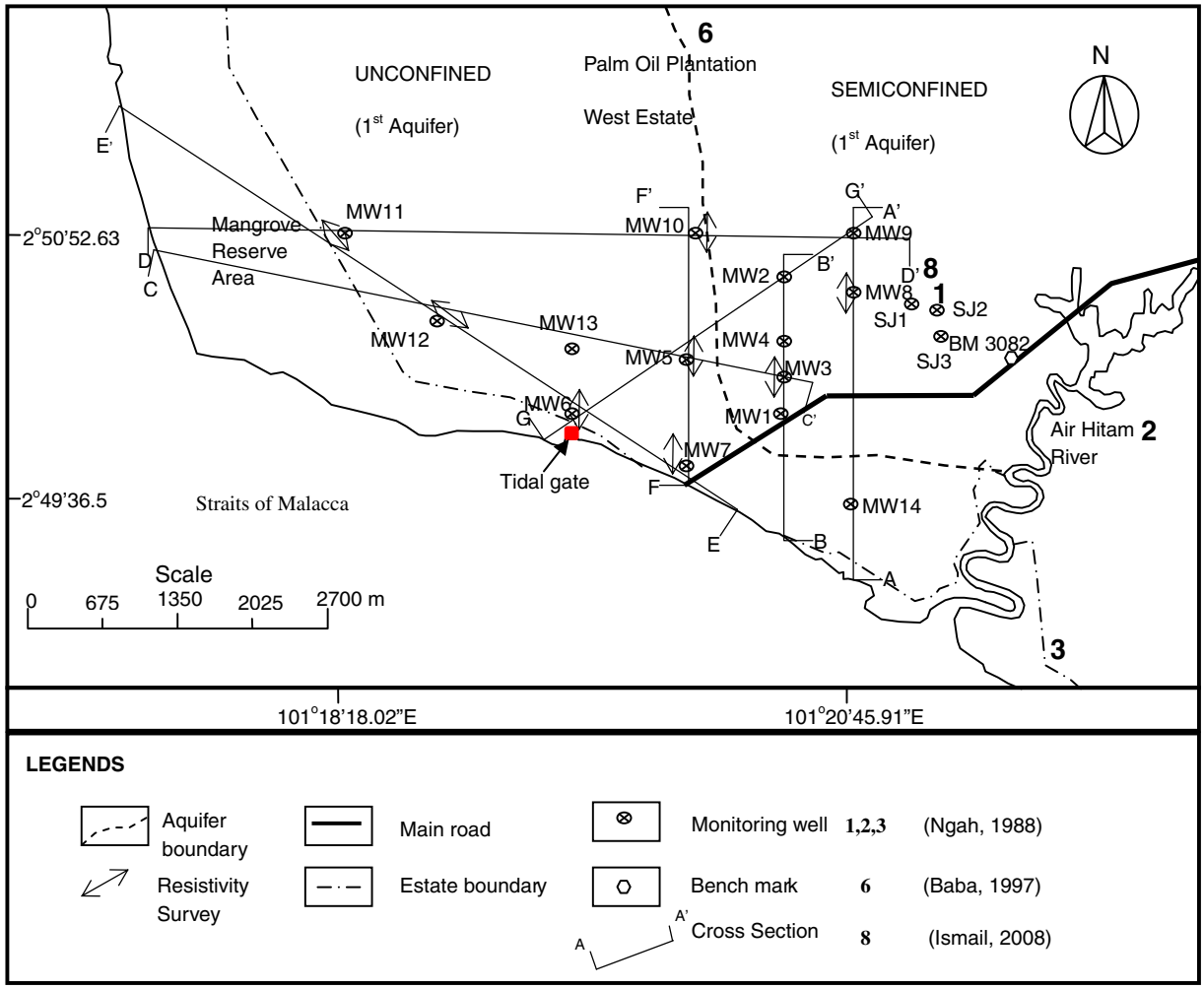

Fig. 3 Locations of monitoring wells, resistivity survey lines, and boundary between unconfined and semi-confined aquifers

This study used TLERT at an ex-promontory land: Carey Island. It identified (via borehole-data, hydro-geochemistry analysis, and land-transformation history) changes in salinity of the tropical island's coastal aquifer system. Its results based a strategy for groundwater exploration of the island.

Area studied

Carey Island, other than being on the west coast of the State of Selangor in Peninsular Malaysia, is separated from the Selangor coast by the Klang River on its north and the Langat River on its east. The study was done in the West Estate of a Sime-Darby Estate Plantation, the exact location was the side that faced seawater (Figs. 1 and 3). JICA and MDGM (2002) report the area's location in the Langat River Basin (Fig. 1), which has two monsoons a year: the northeast, and the southwest. The northeast monsoon is from November to March, and the southwest monsoon is from May to September. Rainfall intensity varies, most of the rain falling in April and November, mean 280 mm. The least rain falls in June; mean 115 mm. Wet seasons are in the monsoons' transitional periods: March to April, and October to November. Monthly rainfall then averages 180 mm, annual precipitation about 2,400 mm (JICA and MDGM 2002). From analysis of Carey Island's local precipitation events and monthly rainfall data from 2000 to 2010, two seasons can be deduced (Fig. 4): wet (August to December, mean 280 mm) and dry (February to March, mean 150 m).

The island's area totals 16,187.45 ha, representing about 6% of Langat Basin. The land is mainly palm oil plantation (10,521.84 ha) and forest-mangrove reserve (1,876.85 ha); the rest are state land and settlements (Golden Hope Plantation Berhad 2006). Population estimate is 10,000, comprising estate workers, locals, and aborigines (Fig. 1).

Hydrogeology

Suntharalingam and Teoh (1985) report the area's underlying Holocene-age marine sediments existing over most of West Peninsular Malaysia's coast referred to as the Gula Formation. The sediments comprise gray clay and sand, minor gravel with traces of fragmented shells, and peaty materials. No indication of exposed outcrop on the island, except for a granitic rock outcrop at Jugra Hills by the Langat River. Studies by Baba (1997), Tahir and Abdul Hamid (2003), and Ismail (2008), on wells 96 to 185 m deep, show its aquifers as being semi-confined.

Other studies have yet to explain the hydrogeology work done west of the area (Figs. 1 and 3). This work built, between March and May 2009,

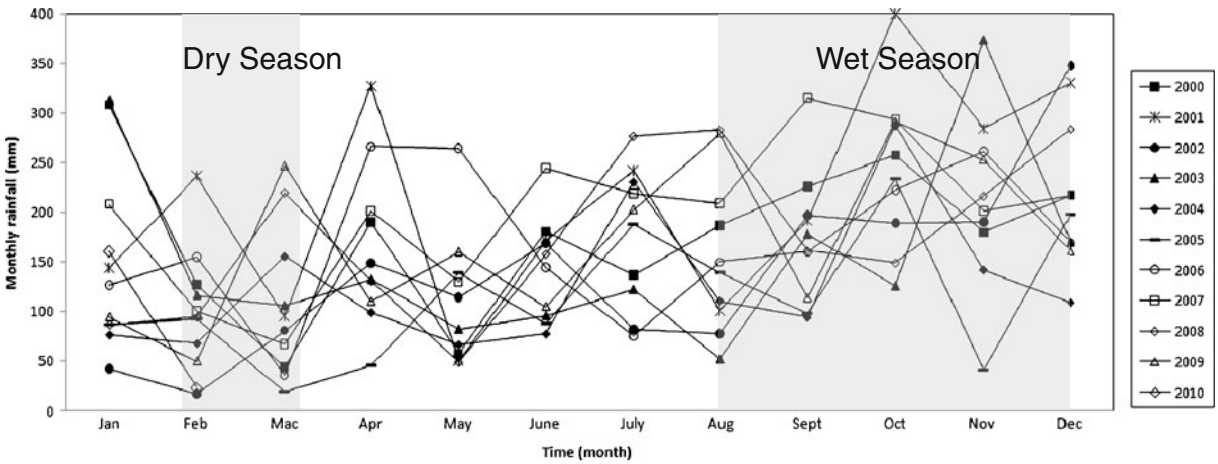

Fig. 4 Dry and wet seasons deduced from analysis of Carey Island's 2000–2010 monthly rainfall data; Department of Irrigation and Drainage (DID), Malaysia, 2009–2010, West Estate Carey Island Rainfall, Station No: 2913121

14 monitoring wells (Fig. 3) that were 40, 50, and 80 m, filling gaps left by preceding studies. The wells faced the Straits of Malacca where saltwater was assumed to hit. They were constructed, and then developed. Rotary-wash boring drilled the boreholes, and soil samples were collected for visual examination and laboratory test experiments (BS1377 1990) to determine physical properties. Bailer and suction pump removed trapped sediments, so good data for groundwater quality and quantity could be obtained (Figs. 2 and 3).

Analysis of the monitoring wells' borelogs shows the area's lithology as being Quaternary alluvium sediments reaching beyond 80 m depth. Quaternary alluvium sediments comprise alternating layers of gravel, sand, silt, and clay. Figures 5, 6, and 7 are cross-sections of the area's hydrogeology. Two aquifers were found 80 m down in the Quaternary sediments. At distances up to 1.5 km from shoreline, the first aquifer, 10 to 60 m deep, could be categorized as being unconfined. Beyond 1.5 km, the first aquifer showed semi-confined characteristics (Fig. 4).

Borelog information for MW1, MW2, MW3, MW4, MW8, and MW9 (Figs. 1 and 3) showed presence of semi-confined aquifers. In the first semi-confined aquifer, thickness of the uppermost semi-impermeable layer varied from 27.00 to 31.50 m below ground surface. The soil was light gray, marine, silty clay. The semi-impermeable layer overlying the first semi-confined aquifer comprised fine-to-coarse light-gray sand and gravel. Thicknesses of the semi-confined aquifers ranged approximately from 20 to 30 m (see Figs. 5 and 6). Borelog information from MW1 and MW2 (Fig. 6) showed depth of the first semi-confined aquifer reaching between 60 and 66 m. The first semi-confined aquifer overlay a thin semi-impermeable layer 3 to 5 m thick, separating the first semi-confined aquifer from the second semi-confined aquifer (Figs. 5 and 6). Thickness of the second semi-confined aquifer was unknown, owing to borehole-depth limit.

Analysis of borelogs for MW5, MW6, MW7, MW10, MW11, MW12, MW13, and MW14 revealed the following information: that the first unconfined comprised fine-to-coarse light-gray sand and gravel, impermeable materials (silt and clay), and fragmented shells (which confirmed that the layers were deposited by a marine environment, i.e., the Gula Formation (Fig. 7). Thicknesses of the first unconfined aquifers ranged from 10 m to

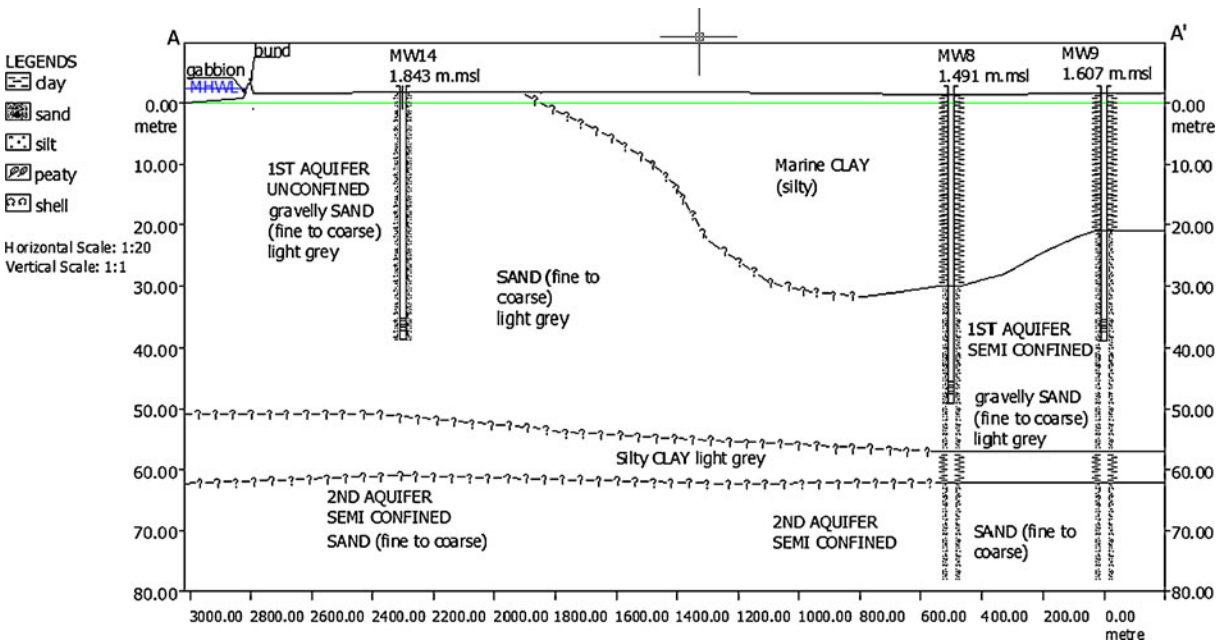

Fig. 5 *A–A′* cross-section of the studied area's subsurface profile showing unconfined and semi-confined aquifers

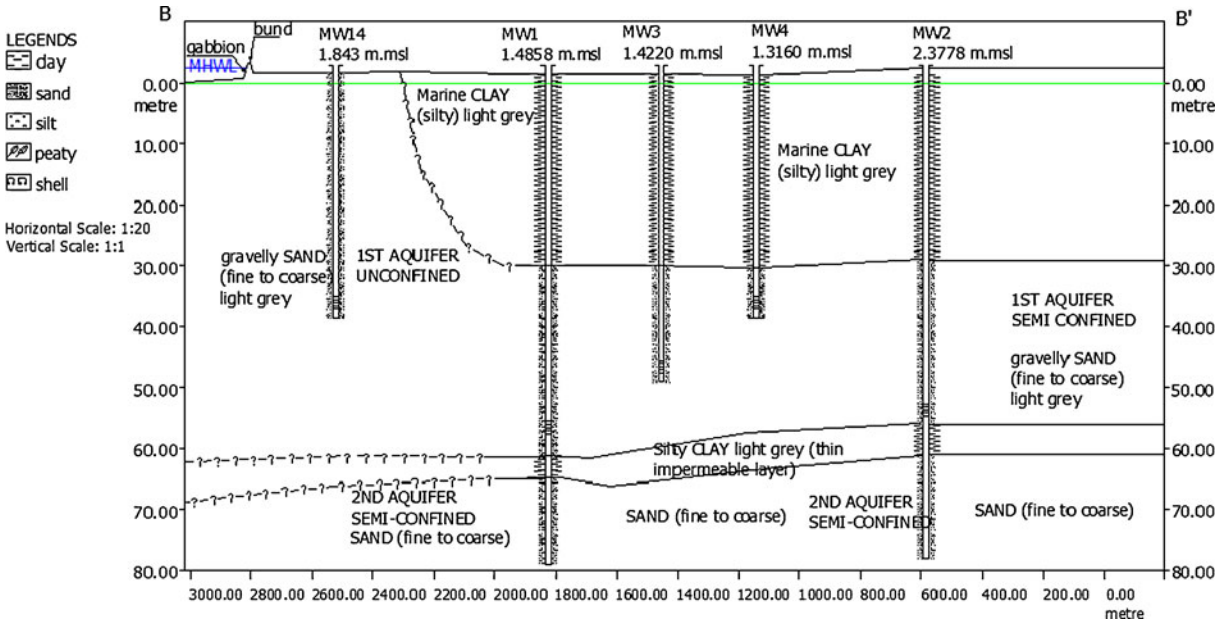

Fig. 6 *B–B′* cross-section of the studied area's subsurface profile showing unconfined and semi-confined aquifers

40 m. Borelog data from MW1 and MW2 (Fig. 5) and 6 (Fig. 3) at the semi-confined aquifer based the prediction that maximum depth of the first unconfined was 60 m. The first aquifer overlay the extended thin semi-impermeable layer of the semi-confined aquifer.

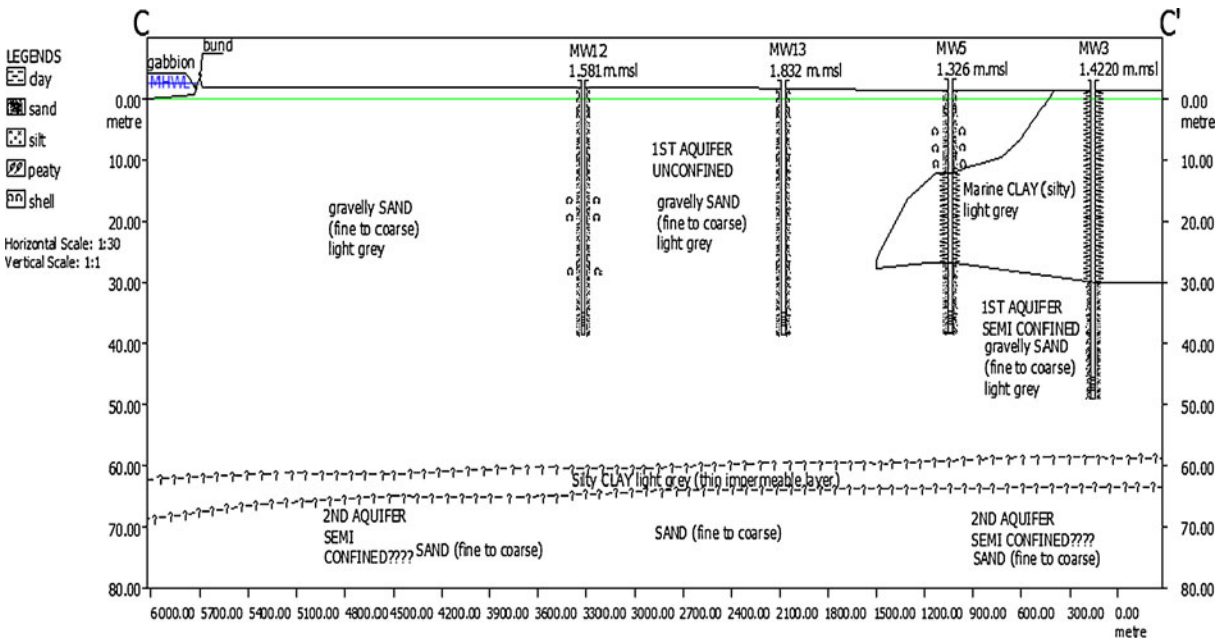

Fig. 7 Subsurface profile of *C–C′* cross-section of the studied area's subsurface profile showing unconfined and semi-confined aquifers. Note that fragmented shells were found at MW12 and MW5 (quaternary alluvium deposit referred as Gula Formation)

The Quaternary alluvium sediment was underlain by granitic bedrock. Depth to bedrock from the drilled borehole (at Kg. Sg. Judah) 30 m away from MW8, was 185 m (Ismail 2008). There had not been groundwater extraction for domestic or economic uses that could have affected the area's rapid fluctuation of groundwater table. Figure 3 shows the boundary between the area's unconfined and semi-confined aquifers (Fig. 5).

Formation of Carey Island

History of the island's formation is based on two theories. In the first, it had been part of a mainland that gradually was disconnected, owing to piracy in the nineteenth century. In the second, it had been promontory, and became an island when the Chinese broke through the little strip of land separating the river and the straits; the rest of the river came about through nature (Golden Hope Plantation Berhad 2006). In the twentieth century, E.V. Carey transformed the mangrove-preserved island into rubber-tree (which later turned into palm oil) plantation. To irrigate the area, dykes were excavated, and drainages, bunds, and tidal gates constructed to control saltwater intrusion. Its history gives some idea on the island's post-land-transformation hydrology and hydrogeology.

A significant hydrological change is the cut-off of the surface runoff that had flowed to the area from the Hulu Langat upper catchment. The island is almost flat and there are no catchments to store precipitation freshwater. The nearest catchment is Jugra Hill, outside the area studied. Drainage for its agricultural activities has always been saline or brackish because freshwater can not infiltrate through the surface runoff or from the drainage of the upper stream. Some locations north of Carey Island show distinct topography, owing to its two-meters-below-sea-level location (Golden Hope Plantation Berhad 2006), a factor contributing to the area's drainage-system salinity or brackishness. Freshwater is believed to come from the mainland's base flow or through direct infiltration at an unconfined aquifer on the island. Shortage of freshwater entering the island through surface hydrology affected its hydrogeology. Carey Island, on the edge of Langat Basin (Fig. 1), furthermore does not receive upper-catchment surface water freshwater (Figs. 6 and 7).

Methodology

Groundwater monitoring was done once or twice a week, starting August 2009 until June 2010. After 2 h (maximum) of daily high tide and low tide, groundwater samples were collected from the monitoring wells by using a bailer. Physical parameters such as conductivity, salinity, total dissolved solids (TDS), and temperature were measured by using precision equipment EC300 YSI immediately after sampling. The equipment was calibrated against a standard potassium chloride (KCl) solution of 1.411 mS/cm conductivity. Groundwater samples were on 30 May 2010 collected for hydro-geochemical analysis. Besides groundwater hydro-geochemistry analysis, irrigation water especially near MW12 was analyzed. Physical parameters were monitored and analyzed from June 2010 to September 2010. Hydro-geochemical parameters measured were major cations and anions. Collected groundwater samples were divided, kept in two containers. For cation analysis, the groundwater samples were filtered by Whatman 42 filter paper and preserved with 2% nitric acid (HNO_3). For anion analysis, the groundwater samples were filtered and then preserved at a maintained 4°C. The anion analysis was done within 48 h of collection time. Cations analyzed were sodium (Na), calcium (Ca), magnesium (Mg), potassium (K), and iron (Fe), on the Perkin Elmer Inductive Coupled Plasma Optical Emission Spectrometer (ICP-OES) model Optima 3300RL. Anions analyzed were chloride (Cl^-), sulfate (SO_4^{2-}), nitrate (NO_3^-), and bromide (Br^-), on Dionex Ion Chromatography model ICS2000. The analyses were done to standard methods (APHA 2005), a five-point calibration quantifying the analyses with correlation co-efficient of the calibration curve between 0.995 and 0.999. Water classification was based on Fetter (2001), and three types were identified: saline (TDS > 10,000 mg/l), brackish (1,000 < TDS < 10,000 mg/l), and fresh (TDS < 1,000 mg/l).

All the station's equipment was used to survey the heights of the 14 monitoring wells and the tide level, both benchmarked to TBM 3082, at 3.0458 m msl. Tide conditions (low- and high-tide increments) were compared with standard national tides (Klang Station; Fig. 1; DSMM 2009, 2010). The Klang Station's datum-level observation for 22 years (1984–2005), was used as references when calculating tide patterns.

Electrical resistivity measurements were performed three times; in August 2009, in November 2009, and in February 2010. Geo-electric survey was via ABEM Terrameter SAS4000 combined with ES10-64 electrode selector. Eight resistivity-image profiles (Fig. 2) were measured across site. For each profile, 61 electrodes were pegged 5 m apart and connected to the cable joined to the ES10-64 electrode selector along 400 m of ground surface. The survey line traverses were oriented N–S. Wenner array was chosen for the resistivity traverses because it gives a dense near-surface-cover of resistivity data. Also, it gives (as horizontal structures) good vertical resolution and clear images of groundwater, saltwater intrusion, and sand-clay boundaries (Hamzah et al. 2006). Data gathered were interpreted by Res2Dinv software of Loke et al. (2003) which provided an inverse model that approximated actual subsurface resistivity distribution. The program divided into a number of rectangular blocks, the two-dimensional model used in the subsurface (Loke and Barker 1996). To minimize difference between measured, and calculated, apparent resistivity values, the blocks' resistivity values were adjusted iteratively. Calculation was by finite-difference method of Dey and Morrison (1979). Resistivity field data collected through Wenner array from individual survey lines were inverted individually to generate a 2D Wenner resistivity model. The inversions were performed on an AMD Athlon(tm) 64 X2 Dual-Core Processor TK-57 1.90 GHz with 3.00 GB RAM. An initial model was produced, from which a response was calculated and compared with measured data. The model was then modified, to reduce differences between response and data. Differences were quantified as root-mean-squared (RMS) errors. The process continued iteratively until RMS error fell to within acceptable limits, usually below 5%, or until change between RMS values calculated for consecutive iterations became insignificant (Awni 2006). The model with the lowest possible RMS error, however, is not always the most appropriate one as it can show unrealistic variations in the resistivity model (Loke 2010b). Finite-difference method was used as the data did not include topography. Given the site's near-flatness, the topography was concluded as being not significantly affecting its resistivity models.

2D-inversion techniques are common and often acceptable in assessing resolution and in determining data-set limitations (Dahlin and Loke 1998). Resistivity of fresh groundwater varies from 10 to 100 Ω m depending on dissolved-salt concentration. Seawater's low resistivity (<0.2 Ω m) is due to its high salt-content (Loke 2010a), making resistivity method an ideal technique for mapping of saline–freshwater interface. Note that resistivity of alluvium ranges from 10 to 800 Ω m depending on soil type.

As mentioned, geo-electric imaging surveys can be used for space and time. Loke (2010b) showed that accurate time-lapse resistivity measurements can be obtained if apparent resistivity values had been accurately obtained. From earlier attempts at measuring time-lapse resistivity, half the data obtained comprised negative readings, resulting in inaccurate apparent resistivity data. Negative readings were due to poor grounding of injected electrical current (ABEM 2009). Extreme tropical-rainforest climate exhibits high temperatures that can reach 36°C in the afternoon, which also causes poor grounding especially to soil containing unsaturated sand material. For good apparent-resistivity data, a few steps were taken for good ground-contact and current injection, including hammering down the electrodes to deeper than 0.3 m, maintaining sufficient moisture for ground contact by using a formulated solution (bentonite polymer solution mixed with salt solution), and by using a more powerful battery (current injection > 60 Ah; ABEM 2009). More than 90% of apparent-resistivity data then obtained showed relative standard deviations of less than 1%, through two-stack measurement which indicate highly stable repeated measurements. In 1 day, five to eight readings were taken at hourly intervals to observe resistivity changes.

Groundwater samples were collected every hour to calibrate geo-electric images against geochemical data.

Data processing and interpretation

Electrical-resistivity data were processed and interpreted by commercial Res2Dinv software, which allowed, via use of the dongle, its full use in analyzing time-lapse resistivity. This study used a joint-inversion technique to minimize possible distortions of sections showing relative changes in subsurface resistivity (Loke 1999). The technique used the inversion model from the initial data set to limit inversion of the later data sets. The time-lapse inversion constraint used was the least-square-smoothness type, which showed the images' smooth changes in domains of space and time. Sequential inversion was used because the section models showed very large resistivity contrasts; the lowest resistivity values ranged from 0.3 to 0.5 Ω m, the highest ranged from 18.0 to 20.0 Ω m (Figs. 22, 23, 24, 25, 26, 27, 28, and 29). In sequential inversion, full inversion of the first data set was for between one and about five iterations. The model for the first data set's final iteration was then used as reference model for inversion of later data sets, which started only upon completion of inversion. The first inversion model data set remained a reference inversion model for the second data set and for subsequent other data sets. The time-constraint weight was 3.0. Output of each resistivity measurement series model is presented here as percent change of resistivity, obtained through Eq. 1:

$$\frac{(x_i - x_1) \times 100}{x_1} \tag{1}$$

where x_i is the measurement series at time i and x_1 the initial series.

The initial series, x_1, presented as reference model from inversion results of the first data set, remained forever a reference model in this equation. Measurement series at time i represented other data-set inversion models at various times. If the output had a negative value, resistivity in the measurement series had more TDS than in the initial series. If the output value was positive, resistivity in the measurement series had less TDS than in the initial series. Salinity changes possibly affected TDS values.

Results

Hydro-geochemical parameters

The samples were analyzed for major cations and anions. Table 1 lists results, which show sodium (Na) and chloride (Cl) exceeding 70% of measured TDS. Dominant contents of sodium and chloride show seawater intrusion to be the source of salinity (Samsudin et al. 2008; Pujari and Soni 2008). Seawater intrusion was thus confirmed as causing the site's salinity.

Findings of previous studies showed no possibility of groundwater existing in deep semi-confined aquifers, except where shallow aquifers form freshwater lens. This study's latest hydrogeology information creates focus on new potentials of unconfined aquifer. Season and tide effects on quantity and quality of groundwater in unconfined aquifer were studied (Figs. 8 and 9). Each of the monitoring wells in the unconfined aquifer was equipped with a 2 m screen, 34 m high aboveground. As the site's topography was assumed flat, measurement of the physical parameters was assumed to be at the same datum.

Figure 8 shows changes to the groundwater wells' water table, whose level increased in the wet season and decreased in the dry season. This shows that the unconfined aquifer responded more quickly to the local seasonal conditions than to Langat Basin seasonal conditions. The finding confirms that groundwater recharge at the site relies totally on local precipitation rather than on base flow from mainland. Overall, high tide did not affect monitoring-well water table much except in MW7 (which was very near the coast); at highest tide, water-table fluctuation was more significant in MW7 than in the other wells. The highest (depth 0.95 m msl) water table in the system was in MW12, and the lowest (depth 0.1 m msl) was in MW10. TDS measurements for both wells differed markedly; MW12 had the lowest TDS below saline level, MW10's reaching a maximum of 25,000 mg/l; Figs. 8 and 9. The huge difference was

Table 1 Results for hydro-geochemical analysis of drain-water and groundwater; water samples taken on 30 May 2010

Well/Drain ID	Na	Mg	Ca	K	Fe	Cl^-	SO_4^-	NO_3^-	Br^-	Fl^-	Total mg/l	TDS, mg/l	NaCl/TDS %	Type of Aquifer based on the screen level
MW1	2799	377	174	115	5	6726	367	<1	<1	<1	10563	11100	86	Semiconfined
MW2	1860	299	143	89	<1	5872	45	<1	<1	46	8354	8450	92	Semiconfined
MW3	5560	707	195	189	<1	12298	241	<1	<1	<1	19190	21820	82	Semiconfined
MW4	5236	683	179	189	<1	9624	<1	<1	<1	<1	15911	20940	71	Semiconfined
MW5	5545	756	237	198	<1	10915	<1	<1	<1	<1	17651	21770	76	Semiconfined
MW6	2959	259	81	128	<1	4560	227	<1	<1	<1	8214	10410	72	Unconfined
MW7	5504	767	225	212	<1	11421	99	<1	<1	<1	18228	22210	76	Unconfined
MW8	4868	517	144	177	<1	8348	65	<1	<1	<1	14119	17960	74	Semiconfined
MW9	2130	357	175	97	<1	6126	78	<1	<1	<1	8963	9230	89	Semiconfined
MW10	4756	495	98	129	<1	15670	159	<1	<1	<1	21307	24650	83	Unconfined
MW11	2335	406	189	82	<1	5768	85	<1	<1	<1	8865	9470	86	Unconfined
MW12	2408	189	75	106	<1	3486	183	<1	<1	<1	6447	8330	71	Unconfined
MW13	2657	234	74	89	<1	4109	99	<1	<1	<1	7254	9570	71	Unconfined
MW14	4232	477	108	195	<1	7244	173	<1	<1	<1	12429	15670	73	Unconfined
Drain water MW12	494	79	33	8	3	876	574	<1	<1	<1	2043	2300	60	–

due to the different rates surface water recharges groundwater. MW12 received more surface water recharge than did MW10. Figure 9 shows groundwater to be saline in MW6, MW7, MW10, and MW 11, but below saline in MW12 and MW13.

MW12's high water table and low TDS suggest its surrounding area to be ideal for fresh groundwater to occur. Long-term monitoring of tide-caused TDS shows that (especially at MW12) most TDS values are slightly higher at high tide

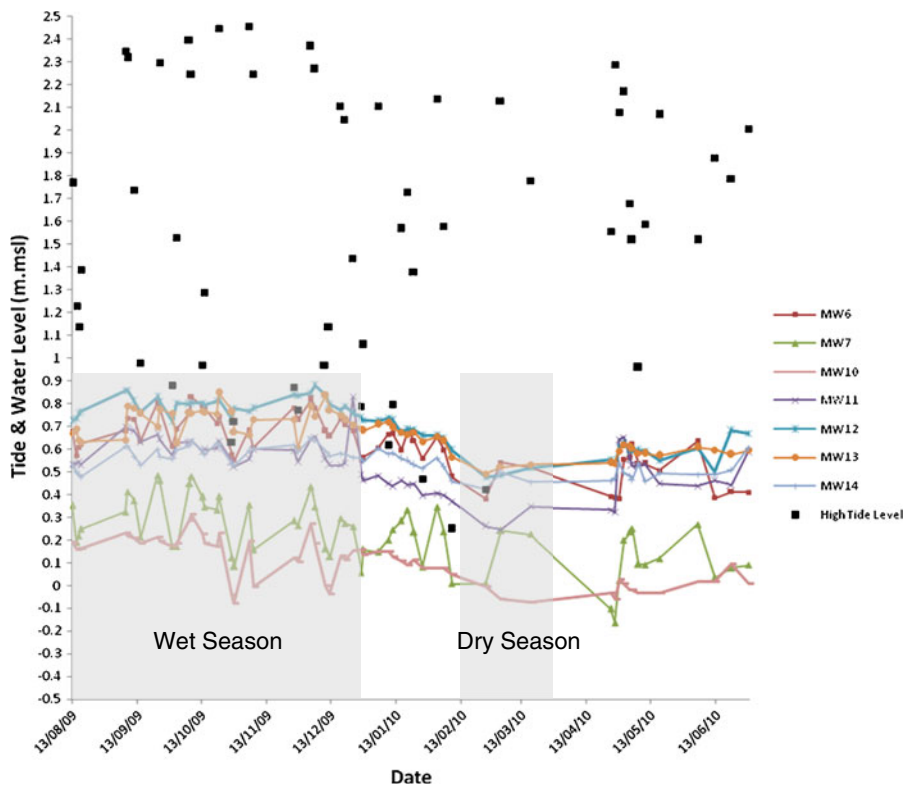

Fig. 8 Most of the groundwater tables of the monitoring wells were influenced by seasonal variables, except for MW7 (influenced by tide)

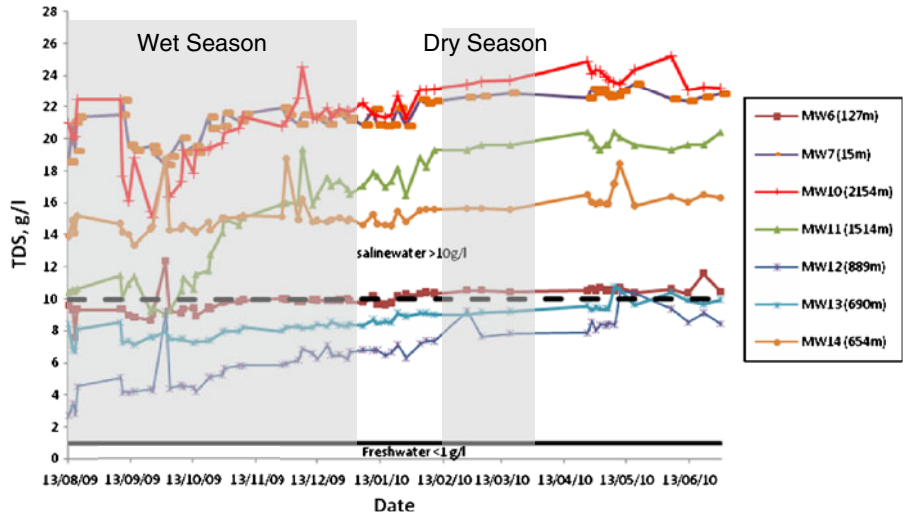

Fig. 9 Plot of TDS against time (in days), for seasonal variables and at unconfined monitoring wells

than at low tide (Fig. 10). This type of data, however, for 34–36 m water-sample depths, is spatially limited, so to define the phenomenon, TLERT and land transformation history was used along with conventional method (Fig. 8).

Correlation between earth resistivity and groundwater quality

The correlation was found in geo-electrical study on seawater intrusion (Ebraheem et al. 1997; Wilson et al. 2006; Sherif et al. 2006; Pujari and Soni 2008). Interpretation of resistivity data is difficult, however, for salinity changes that are due to interaction between seawater intrusion and fresh groundwater and to background resistivity; the most challenging is attempting to link earth resistivity to groundwater type (fresh, brackish, or saline). Pore fluid is a mixture of fresh water and saline water, with various proportions of salinity concentration. It is embedded in the pores of the host soil, whose various resistivity values correspond to its mineral composition. Attempting interpretation of groundwater type is thus almost impossible (Figs. 9 and 10).

In this study, more than 80% of the resistivity images (Figs. 11, 14, 15, 16, 17, 18, 19, and 20) show low resistivity (<3 Ω m). Exceptions are the ones for MW6 (Figs. 12 and 13) and for MW12

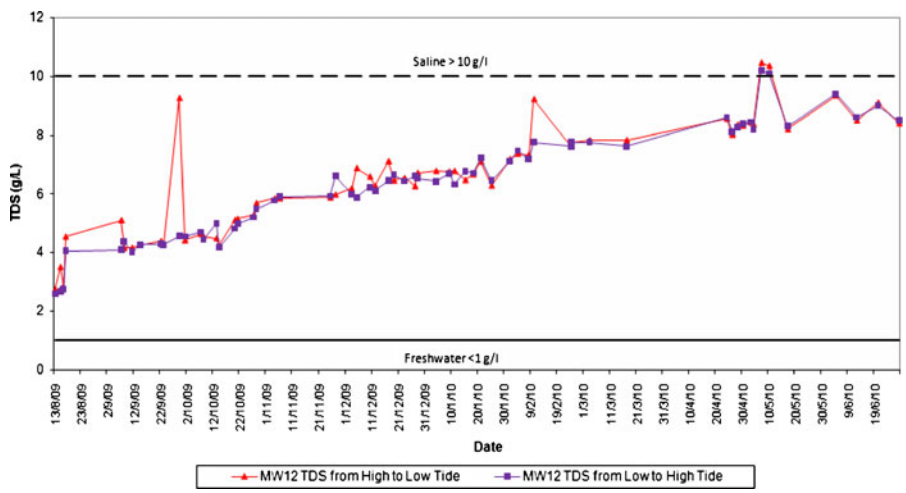

Fig. 10 MW12 TDS values slightly higher at high tide than at low tide

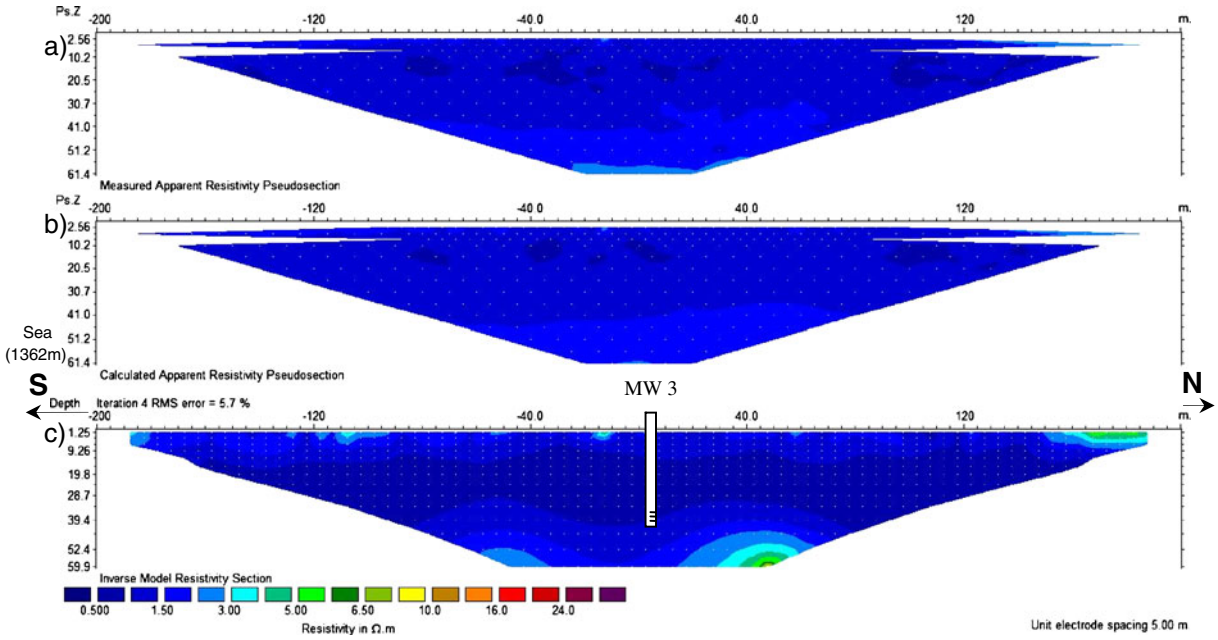

Fig. 11 MW3 resistivity images, August 2009; **a** measured apparent resistivity (Wenner Array), **b** calculated apparent resistivity, and **c** inverse model resistivity

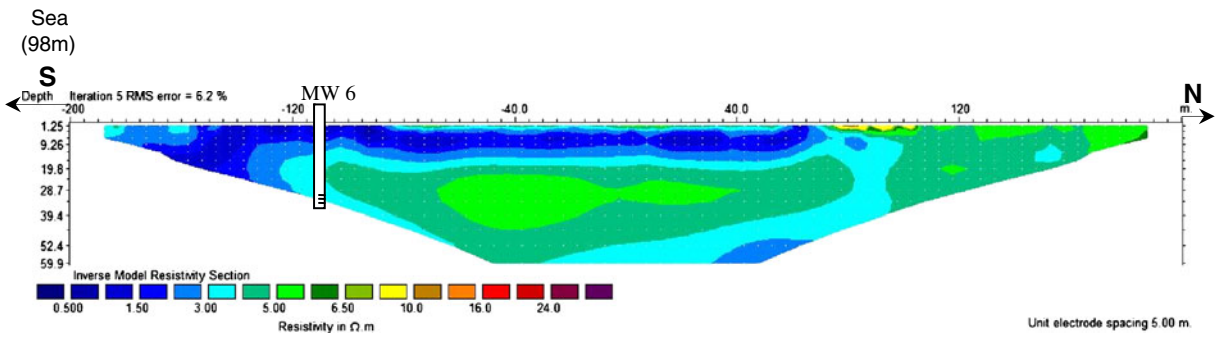

Fig. 12 MW6 resistivity image, August 2009

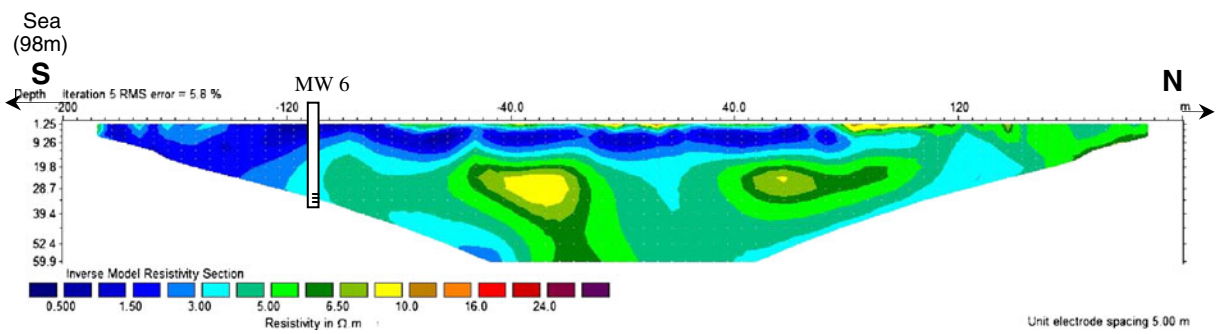

Fig. 13 MW6 resistivity image, November 2009

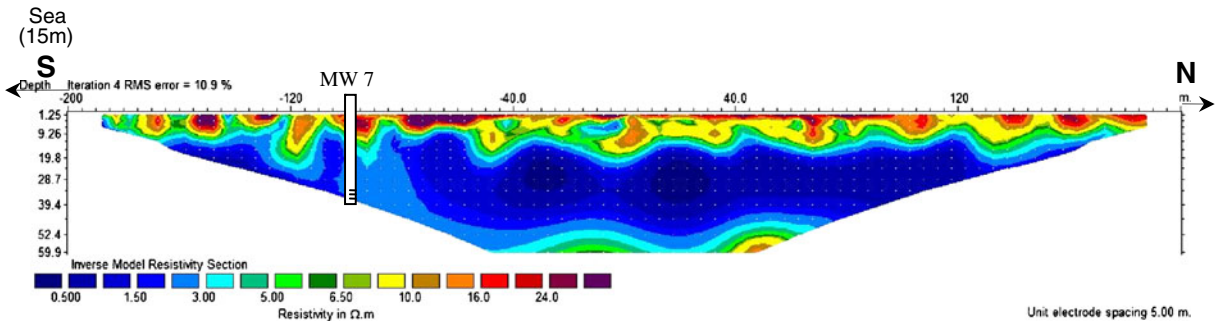

Fig. 14 MW7 resistivity image, August 2009

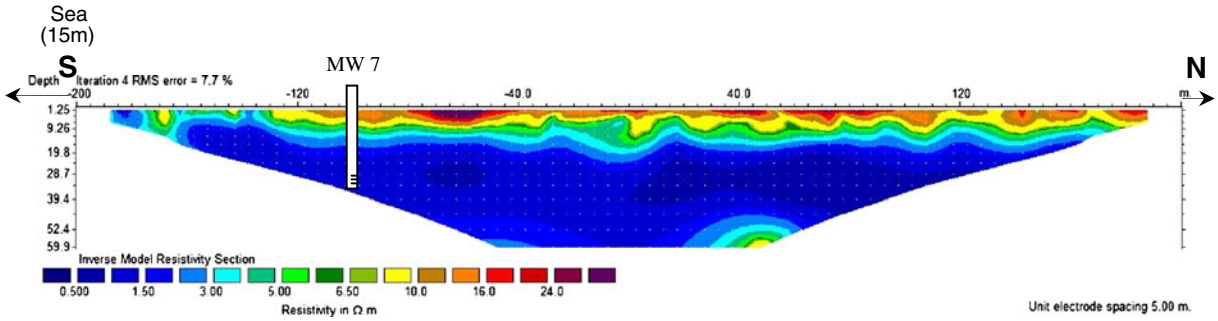

Fig. 15 MW7 resistivity image, November 2009

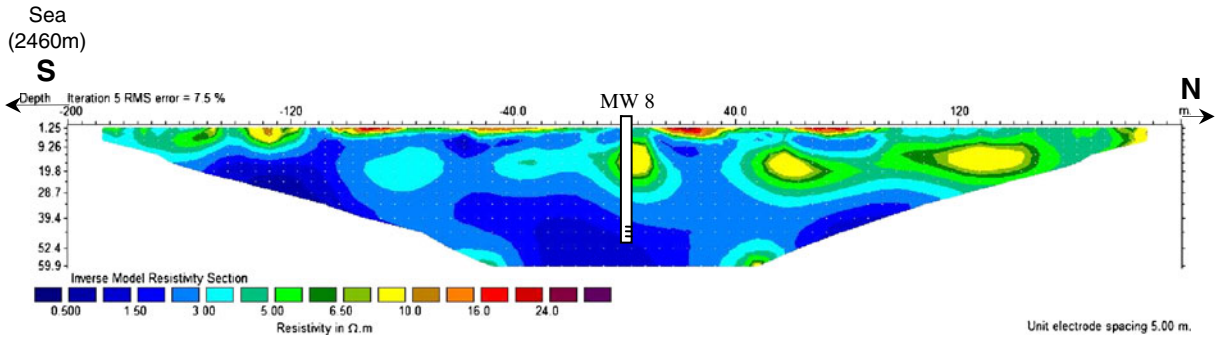

Fig. 16 MW8 resistivity image, August 2009

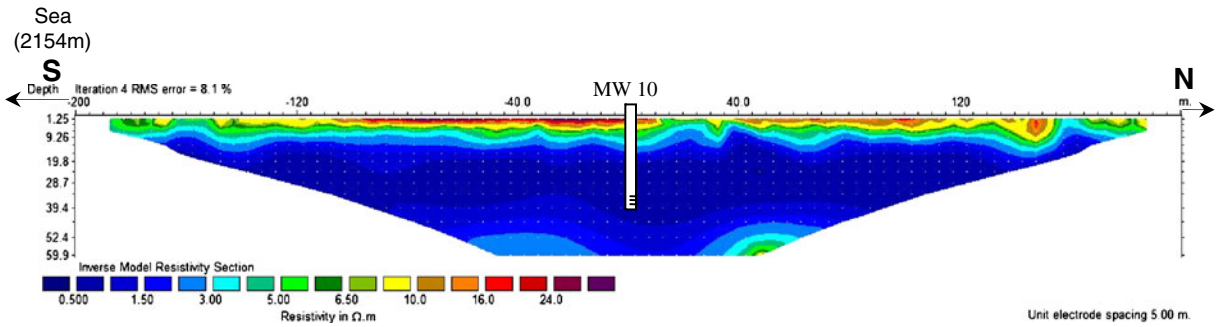

Fig. 17 MW10 resistivity image, August 2009

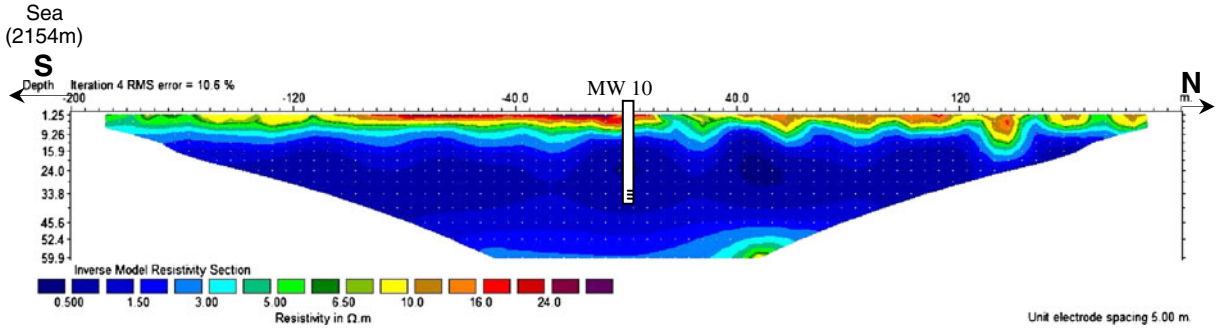

Fig. 18 MW10 resistivity image, February 2010

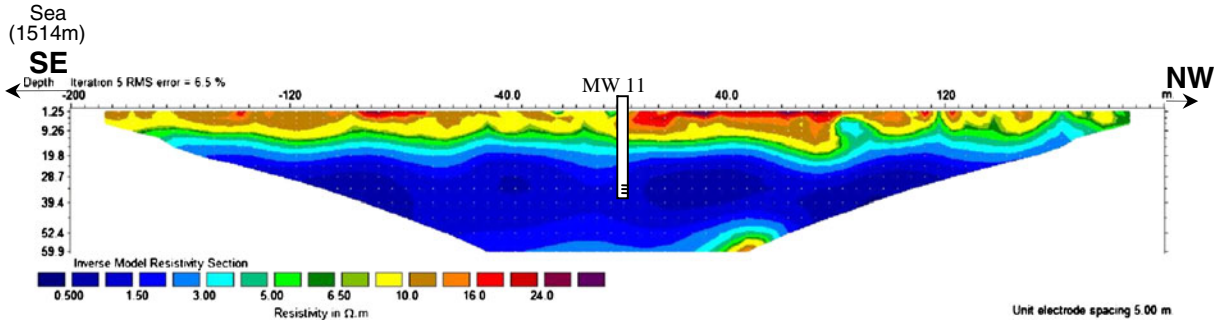

Fig. 19 MW11 resistivity image, August 2009

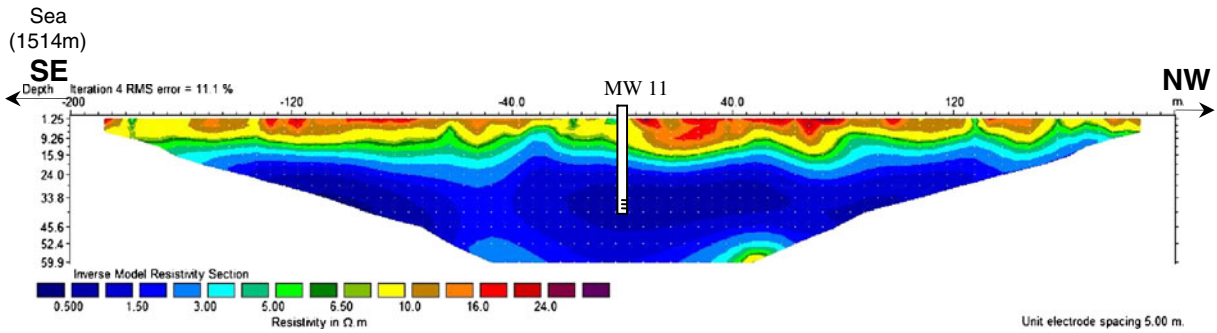

Fig. 20 MW11 resistivity image, February 2010

(Fig. 21). Values of MW6's resistivity profile did not exceed 6.5 Ω m, while those for MW12 ranged from 6.5 to 11.0 Ω m. Resistivity values in preceding studies had a wider range, 0–1,000 Ω m (Wilson et al. 2006), and 0–2,500 Ω m (Pujari and Soni 2008). Wilson et al. (2006) used formation factor to derive bulk earth resistivity and pore-fluid resistivity to classify water types. Pujari and Soni limited the resistivity band, from nearly 0 to 3.0 Ω m (interpreted as seawater intrusion).

Preliminary assumptions were derived from this study. Very low-resistivity values (∼0–3.0 Ω m) were interpreted as indicating saline-water zone. Low-resistivity values (3.0–11.0 Ω m) indicate possible mix of fresh water and seawater in the pores. The alluvial Quaternary comprises homogenous water-bearing sands and the occasional gravel (both attributed to a large volume of pore fluids), contributing to volumes of groundwater flowing through the pores. This study's resistivity measurements thus were probably more influenced by pore-fluid than by mineral composition of soil, and so resistivity images of the water types were more apparent. Concentration of dissolved ions in pore fluids is important for control of groundwater's electricity-transmitting ability (Sherif et al. 2006). Another factor contributing to low resistivity is hydraulic force, which is more dominant in seawater intrusion than in freshwater (whose limited recharge on Carey Island was caused by land-use transformation; Figs. 11, 12, 13, 14, 15, 16, 17, 18, 19, 20, 21).

Ebraheem et al. (1997) and Sherif et al. (2006) stated that empirical relationship between geochemistry and geophysical methods could be derived when ions dissolved in pore fluid rather than in host soil were more apparent in the electrical images. Findings of early research on use of the empirical relationship as showed by resistivity-image data could be used in this study. For empirical relationship between geochemistry and geophysical information, geochemistry data from nine monitoring wells and resistivity measurements from nine transverse geo-electric data were used. Procedures for obtaining these relationships are described by Cartwright and McComas

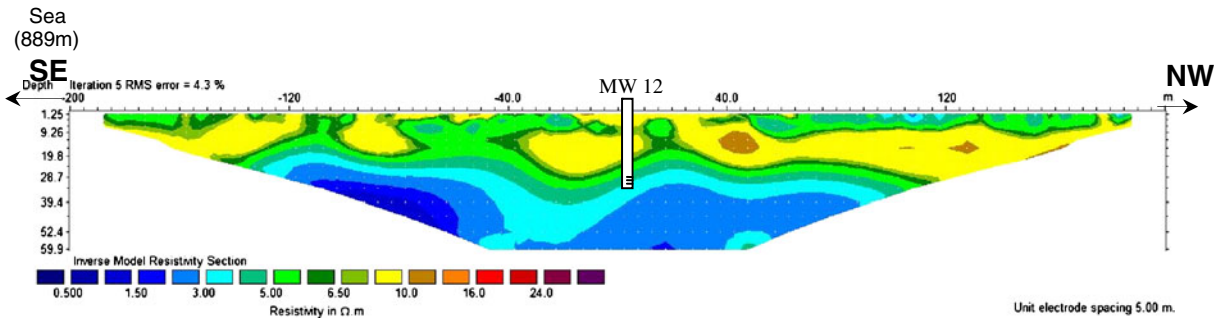

Fig. 21 MW12 resistivity image, August 2009

Table 2 Geo-electrical and hydro-geological data used for empirical relationships between earth resistivity and water resistivity and between TDS and earth resistivity

Well ID	Ground water table depth (m msl)	Water conductance (μmho/cm)	Soil conductance (μmho/cm)	Water resistivity (Ω m)	Earth resistivity (Ω m)	Measured TDS (mg/l)
MW4	0.281	41,745	5,671	0.2395	1.7633	25,420
MW10	0.236	38,560	5,441	0.2593	1.8379	23,490
MW3	0.453	34,080	5,253	0.2954	1.9035	20,730
MW7	0.085	32,950	5,082	0.3035	1.9676	19,820
MW5	0.168	28,920	4,957	0.3458	2.0174	18,020
MW11	0.312	27,250	4,547	0.3670	2.1993	16,620
MW8	0.470	17,990	3,526	0.5559	2.8361	10,800
MW6	0.565	14,040	3,103	0.7123	3.2231	8,440
MW12	0.843	9,790	2,545	1.0215	3.9299	5,950

(1968), Ebraheem et al. (1990), and Sherif et al. (2006). Specific conductance of groundwater samples was converted into water resistivity ($\rho_w = 1/\sigma_w$). Soil conductance was derived by inversing earth-resistivity data ($\sigma_s = 1/\rho_e$). All the data (Table 2) were used to obtain empirical relationships; between earth resistivity and water resistivity, and between TDS and earth resistivity.

Water resistivity was plotted as a function of earth resistivity (Fig. 22). The best regression line between water resistivity and earth resistivity indicates the following empirical relationship:

$$\rho_e = 2.8595\rho_w + 1.1066 \quad (2)$$

where ρ_e is earth resistivity, and ρ_w is water resistivity in ohm-meters (Ω m).

Both parameters show good correlation, with $R^2 = 0.9899$ revealing earth resistivity of Quaternary alluvium aquifer (comprising dominantly coarse, medium, and fine, sand, and occasional gravel), and of saturated groundwater, both of which affect salinity. Both the observation and the analysis reaffirm the basis for applying geo-electric method in studying salinity distribution of Carey Island's groundwater system.

Earth resistivity and TDS were also plotted (Fig. 23). The plot's best regression line indicates the following empirical relationship:

$$\log \text{TDS} = -0.2857\rho_e + 4.8657 \quad (3)$$

The relationship derived from Eq. 3, reveals that three types of groundwater can be depicted in the resistivity images: fresh ($\rho_e > 6.5$ Ω m), brackish (3 Ω m $< \rho_e <$ 6.5 Ω m), and saline ($\rho_e < 3$ Ω m).

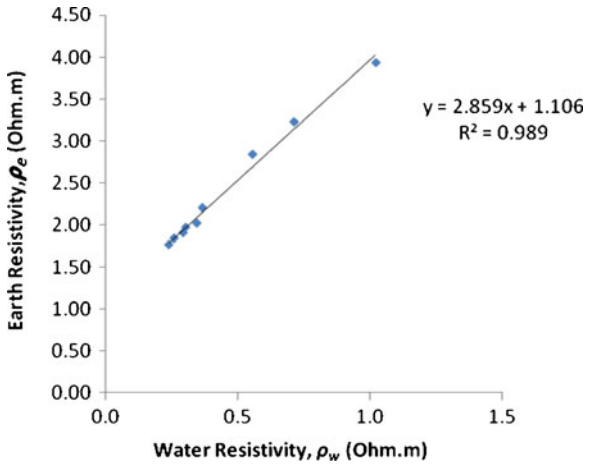

Fig. 22 Earth resistivity versus water resistivity

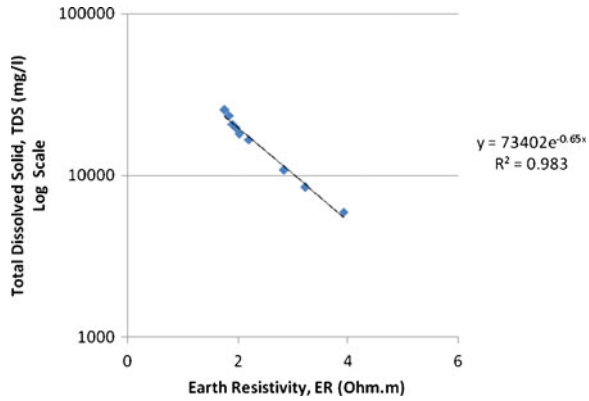

Fig. 23 Empirical relationship between TDS and earth resistivity

Resistivity results

Figures 11, 12, 13, 14, 15, 16, 17, 18, 19, 20, and 21 show the resistivity images of seven monitoring wells. Equation 3 and resistivity images obtained for MW3, MW7, and MW10 (Figs. 11, 14, 15, 17, 18) based the proposition that saline water dominates the existing aquifer system, at depths 10–60 m, with resistivity values 0.5–3.0 Ω m. MW6, which was near an estuary, has its resistivity image (Figs. 12 and 13) showing brackish-water domination along 400 m of resistivity image profile, with resistivity 3.0–6.5 Ω m. At shallow, 2.5–10.0-m depths, saline water dominates, with resistivity 0.5–2.0 Ω m. At those depths, the canals and the estuary are the salinity sources. MW8 resistivity image shows presence of brackish and saline waters, resistivity 0.5–6.5 Ω m.

Resistivity images for MW11 and MW12 show resistivity exceeding 6.5 Ω m, indicating presence of freshwater especially on top of subsurface (Figs. 19, 20, and 21). The freshwater level in MW12 is deeper (30 m) compared with that in MW11 (quite shallow). The images show that distance from saline-water source such as seawater is not the main contributor to salinity pattern on a promontory island. MW3 and MW10, respectively 1.5 and 2.5 km from coast, still showed high salinity levels. Resistivity images show salinity mapping to be almost the same in August 2009 (Figs. 13, 15, 18, and 20).

The area's hydrogeology shows that freshwater recharge from precipitation does not occur upstream or mid-island. Freshwater source is infiltration that happens only at unconfined aquifers; the salinity profile is unconventional, and on a promontory island, not uniform.

Locating freshwater source on a promontory island thus needs an unusual approach. From analyses of resistivity images, MW12's (showing presence of brackish and saline waters beyond 30 m depth), shows potential for freshwater. Investigation of time-lapse resistivity was thus extended, to monitor salinity changes to freshwater aquifer.

Time-lapse resistivity results

Figure 24 shows percent change of MW12's resistivity image, obtained from Eq. 1 at the beginning of the investigation. The image was obtained from the inversion model's subsurface resistivity, which was pre-obtained from data series measured the second time (Fig. 25) and was compared with the initial-data-set reference model (Fig. 26). The second-time data series was obtained after one hour of measuring the reference model's resistivity.

Figure 25 shows, compared with the reference model and especially at subsurface, decreased resistivity after 1-h interval. Especially at the bottom of the image, percentage of resistivity change was in the −20% to 10% range. Figure 27 shows the resistivity image at post-7-h of measurement; the resistivity values are lower than those of the reference and the second-time series. Figure 28 is an image of resistivity-change percentages after 7 h measurement, resulting from comparison between inversion model resistivity values after 7 h mea-

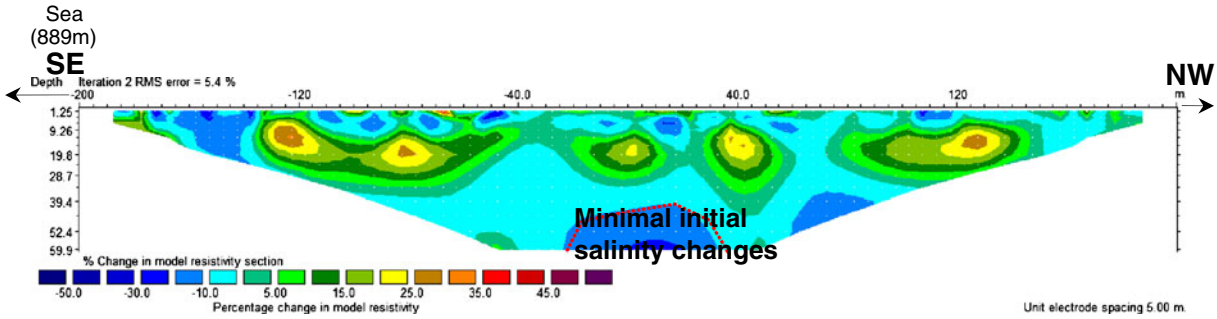

Fig. 24 MW12 resistivity change percentages at 12.00 pm–1.00 pm, 26 August 2009; tide levels 0.448 m msl (12.00 pm), −0.262 m msl (1.00 pm), highest tide 1.778 m msl at 9.00 am

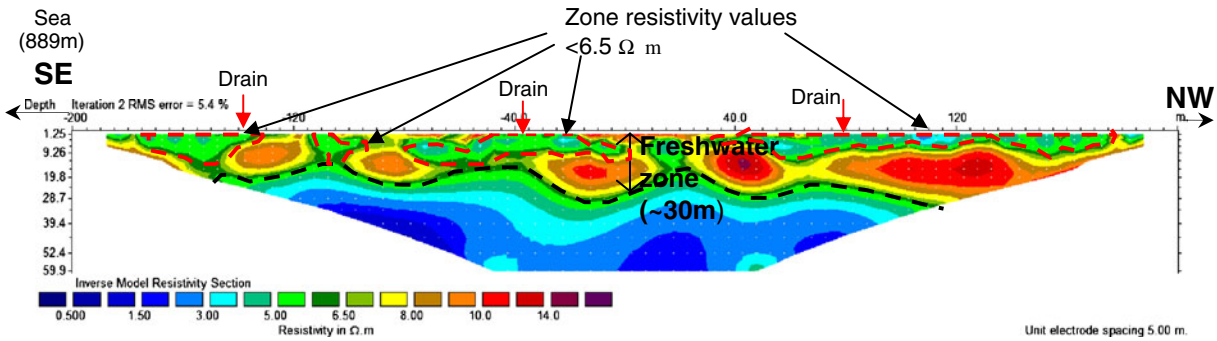

Fig. 25 MW12 second-series resistivity image at 12.00 pm–1.00 pm, 26 August 2009

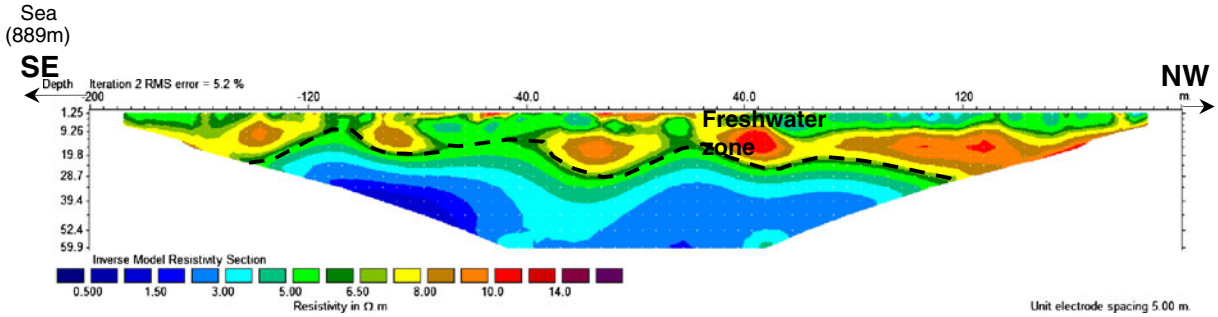

Fig. 26 MW12 reference-model resistivity image at 11.00 am–12.00 pm, 26 August 2009

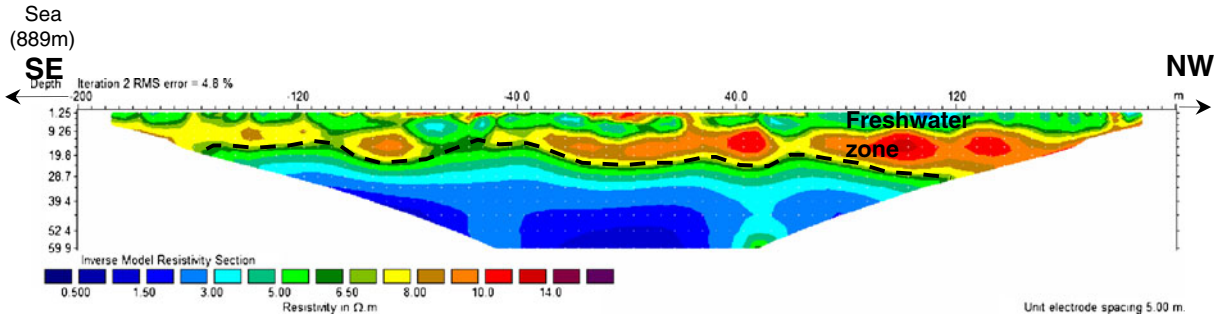

Fig. 27 MW12 seventh-series resistivity image at 5.00 pm–6.00 pm, 26 August 2009

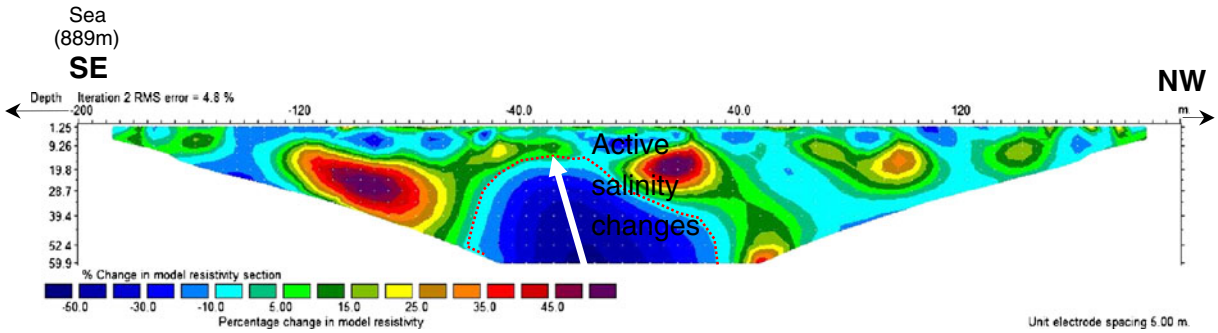

Fig. 28 MW12 resistivity change percentages at 5.00 pm–6.00 pm, 26 August 2009; tide levels −1.022 m msl (5.00 pm), −0.272 m msl (6.00 pm), lowest tide −1.482 m msl at 3.00 pm

surement (Fig. 27) with values of the reference model. Percentages of resistivity change were in the −53.53% to 5% range. Minimal changes observed initially were caused by low tide that occurred 3 h after highest-tide time (Fig. 24). The high percentage observed in the next 7 h was caused by high tide that occurred 2 h after lowest tide, which affected salinity. The widespread salinity was due to effects of tide; for the last measurement's image, 7 h of highest tide.

TLERT studies continued in February dry season, at the same line position in August wet season. Inversion-model data as reference model were obtained at 1 h intervals from beginning of high tide (Fig. 29). Percentages of resistivity change (Fig. 30) were obtained by comparing second-series inversion data (Fig. 31) with those of the reference model. Range of resistivity-change percentages at image bottom was 0–30% (Fig. 30). Figure 32 shows percentages of resistivity image resulting from comparison of inversion model resistivity values after 7 h measurement (Fig. 33) with values of reference model (Fig. 29). Percentages of resistivity change were in the −55% to 0% range. Figure 32 is an image of salinity upward spread, which is bigger than that in Fig. 30. The more-widespread salinity was due to effects of tide; for the last measurement's image, 7 h of highest tide.

Resistivity image for August 2009 wet season shows 30-m-thick aquifer-freshwater lens, which thinned to 20 m in February 2009 dry season (Figs. 25 and 31). The decrease was caused by freshwater recharge (through infiltration of unconfined layer) being greater in the wet season.

Resistivity-image values less than 6.5 Ω m were noted to appear in shallow-subsurface resistivity for both seasons (Figs. 25 and 31). TDS data for drainages nearest to MW12 show values ranging from 1,866 to 2,354 mg/l, as measured between June 2010 and September 2010. Drainage water surrounding the area is high in

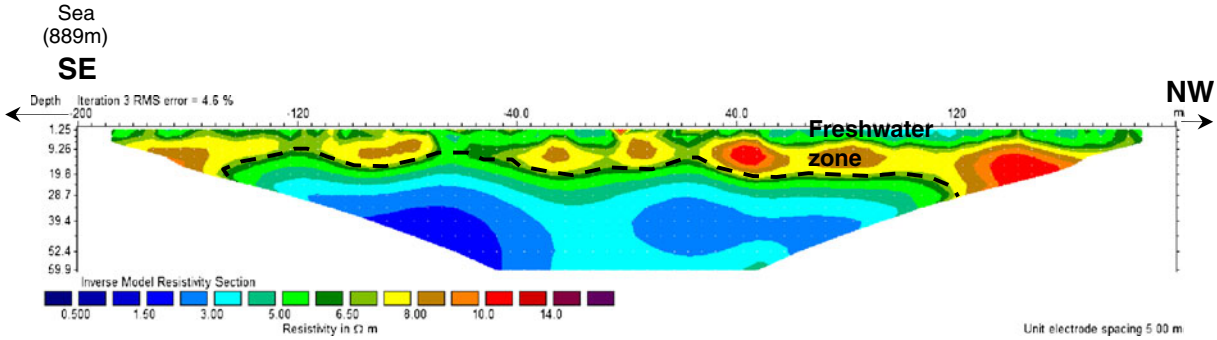

Fig. 29 MW12 reference-model resistivity image at 10.00 am–11.00 am, 10 February 2010

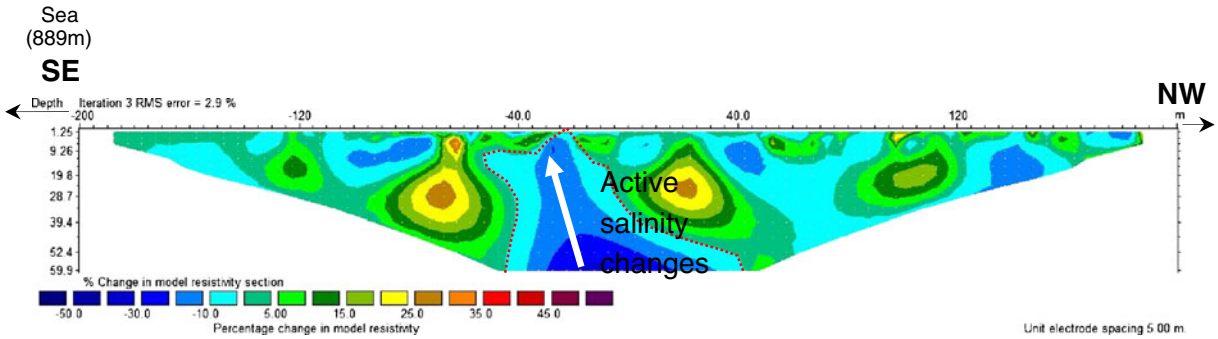

Fig. 30 MW12 resistivity change percentages at 11.00 am–12.00 pm, 10 February 2010; tide levels −1.372 m msl (11.00 am), −1.012 m msl (12.00 pm), lowest tide −1.462 m msl at 10.00 am

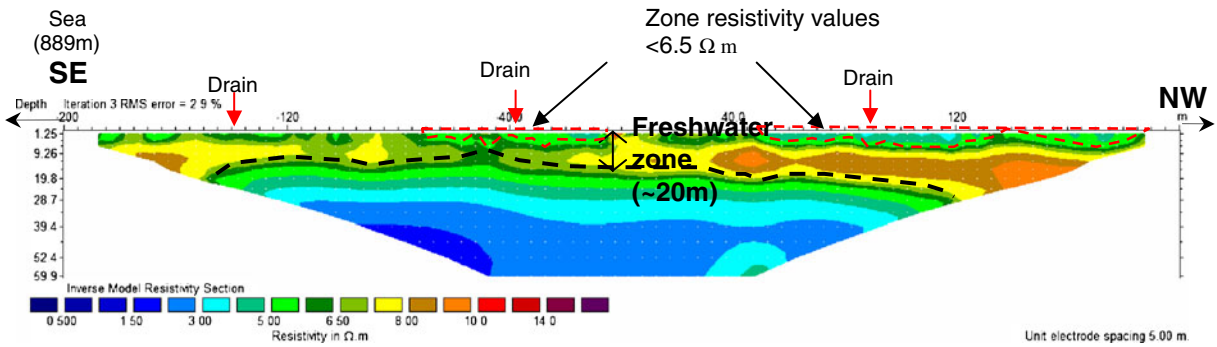

Fig. 31 MW12 second-series resistivity image at 11.00 am–12.00 pm, 10 February 2010

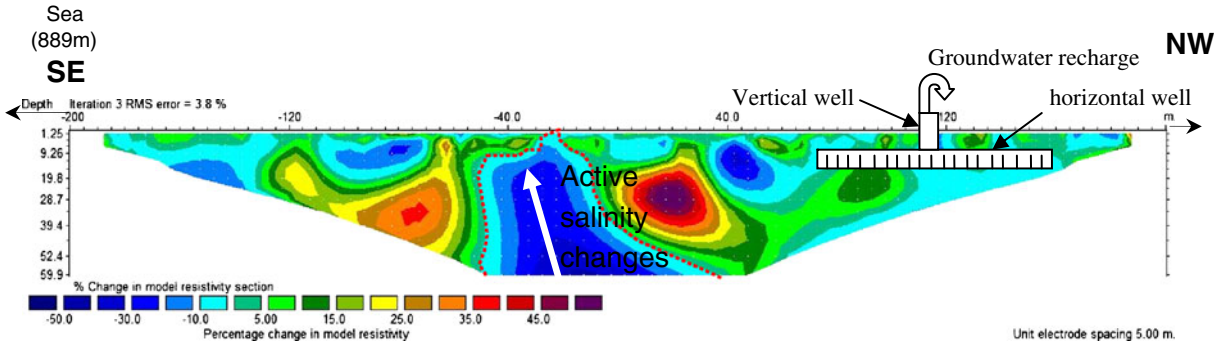

Fig. 32 MW12 resistivity change percentages at 4.00 pm–5.00 pm, 10 February 2010; tide levels 0.528 m msl (4.00 pm), 0.448 m msl (5.00 pm), highest tide 0.528 m msl at 4.00 pm

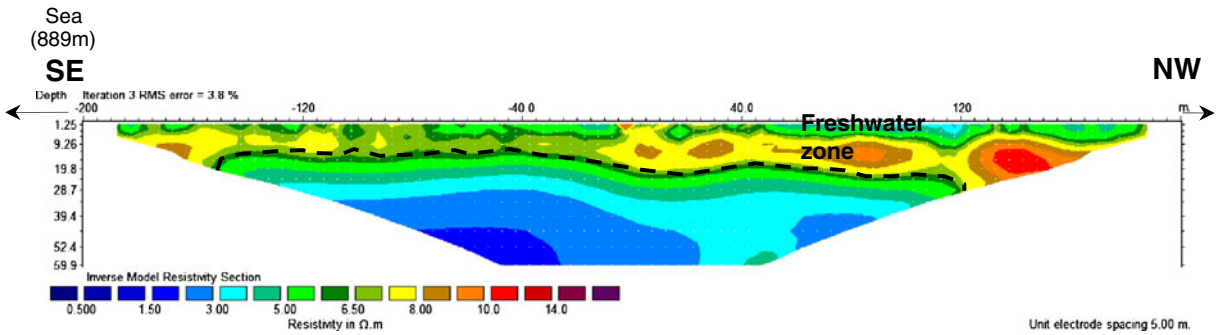

Fig. 33 MW12 seventh-series resistivity image at 4.00 pm–5.00 pm, 10 February 2010

SO_4^-, Cl^-, and Na contents (Table 1). Sodium and chloride represent 60% of the TDS total. Though sampling was out-of-range of resistivity-measurement days, the TDS data could be used as indicator that shallow subsurface was contaminated by infiltration-water drainage. Assumption was made that TDS values for shallow subsurface are slightly more, or slightly less, than TDS values for drainage. By the water-type classification of Fetter (2001), TDS values for shallow subsurface are in brackish-water category. Presence of brackish water in shallow subsurface can also be seen from range of resistivity values, which should be between 3.0 and 6.5 Ω m for brackish-water categorization (Figs. 25 and 31). Further study needs to be done to confirm water type and salinity changes to shallow subsurface. Among required studies are sampling and geochemistry analysis, at to-be-constructed shallow-subsurface monitoring wells.

Salinity-change trend at the bottom of the image for both conditions shows movement from right to left. The trend is believed to have been caused by incremental daily tide passing through the high hydraulic conductivity resulting from high porosity of the material in the studied area (Figs. 24, 25, 26, 27, 28, 29, 30, 31, 32, 33).

Discussion and conclusions

The study shows that salinity changes at an ex-promontory land can be identified via a combination of hydro-geochemistry, electrical-resistivity imaging, and time-lapse resistivity measurement conducted daily and in various seasons, and the resulting information be used to determine a strategy and a policy for groundwater exploration.

Hydro-geochemistry analyses showed high contents of sodium and chloride in all the monitoring wells. The source of salinity in the groundwater system of an ex-promontory land is believed to be seawater. Water-table data and TDS values for the monitoring wells show MW12's potential for freshwater occurrence. Combination of hydro-geochemistry and electrical-resistivity imaging produced an equation for identifying the aquifer's types of water. Resistivity values below 6.5 Ω m show brackish and saline waters. Results from the equation and resistivity image with values exceeding 6.5 Ω m were used to identify freshwater-existence potential.

Resistivity image for MW12 shows it has greater potential for freshwater supply than do the other wells. Thickness of fresh groundwater, as showed by resistivity profile, varied from 20 to 30 m from ground level, overlying saline groundwater according to seasonal conditions. Fresh groundwater for this area came from precipitation and surface runoff and infiltration into soil strata. Density of saline groundwater was greater than density of fresh groundwater, causing saline water to exist beneath subsurface. TLERT studies showed resistivity changes to be wider at image bottom, especially during increased tides, in both season's conditions. Tide increments influenced salinity changes dominantly below freshwater-zone boundary. Incremental tide passing through highly porous materials is believed to have caused high hydraulic conductivity in the active-salinity-

change area. Future work could be measuring of hydraulic conductivity to support the hypothesis.

The island's continuous saltwater pressure to subsurface and limited freshwater recharge indirectly affected its hydrogeology, which had been prone to pressure and limited recharge. Carey Island's transformation from promontory land to island (Golden Hope Plantation Berhad 2006) changed its hydrology and indirectly affected its hydrogeology. The island receives continuous saltwater pressure due to these changes, indirectly resulting in uneven salinity distribution (as showed by previous studies) and causing difficulty in planning a strategy for groundwater exploration. Sources of freshwater recharge of the groundwater system are limited, and exist at saline-water boundary. Time-lapse resistivity measurement can thus be used to identify saltwater-pressure effect, and freshwater-zone thickness. For MW12, located at an unconfined aquifer, active salinity changes were affected by season and tide. Ngah (1988) reports that freshwater lens at semi-confined aquifer can be deteriorated by saltwater intrusion, especially during dry season. Combination with other methods helps more than does one method in describing subsurface-salinity changes that are due to saltwater intrusion.

The results of this study base a strategy for extracting freshwater from unconfined aquifer:

(a) Use of horizontal and vertical wells to prevent induced saltwater intrusion in aquifer.
(b) Placing of production well on the right side of MW12 (Fig. 32), as resistivity image of MW12 shows active salinity changes moving from image bottom right towards image upper left.
(c) Conducting of pumping test and hydrogeochemistry analyses in dry season (February) to ascertain that quantity and quality of groundwater satisfy need and requirement. In dry season, depth of freshwater layer has been found to decrease.
(d) Hand-pumped wells to control rate of discharge of freshwater, to avoid saltwater upcones towards the propose production well.
(e) Finding best-quality freshwater at depths 10–30 m in wet season and 5–20 m in dry season. Level suitable to set well screen is 15 m down, considered a fair level for both seasons.
(f) For more effective irrigation of brackish-water drainage, new tide-control gate should be built. Now, only one tide-gate located near MW6 is being used to irrigate out drainage water from a large portion of the plantation area (Fig. 3). Upper-zone freshwater lens can be assured of less contamination by brackish-water drainage.

Malaysia's Department of Mineral and Geo-Science had used a combination of horizontal and vertical wells for groundwater exploration especially at coastal regions, which are prone to saltwater intrusion (Suratman and Awang 1998). Application of geochemistry data and geo-electric-method borehole data has shown effectiveness of time-lapse electrical-resistivity imaging in defining a strategy for groundwater exploration of complex-hydrogeology ex-promontory land. Such a strategy, at such an area where fresh groundwater is limited, should be investigated further in terms of tide effects, season, and knowledge of the area's land transformation history. A combination of the techniques discussed and the area's environmental history enables drafting of a sustainable strategy for long-term groundwater exploration. Understanding of the study's preliminary results for salinity changes to the groundwater system at the ex-promontory land should help local authorities and villagers plan the area's socio-economics.

Acknowledgement The project has been made possible by a research grant provided by the Institute of Ocean and Earth Science (IOES), project no. TA008-2008A.

References

ABEM (2009). *Instruction manual Terrameter SAS 4000 and SAS 1000. ABEM printed matter 93109* (pp. 1–136). Available from: http://www.abem.se/software.php.

Abdul Nassir, S. S., Loke, M. H., Lee, C. Y., & Nawawi, M. N. M. (2000). Salt-water intrusion mapping by geoelectrical imaging surveys. *Geophysical Prospecting, 48*(4), 647–661. doi:10.1046/j.1365-2478.2000.00209.x. Available from: http://web.ebscohost.com/

ehost/pdf?vid=3&hid=113&sid=f505c08d-d330-4dc5-99bo-df1909144ee2%40sessionmgr109. Accessed 4 January 2009.

Adepelumi, A., Ako, B. D., Ajayi, T. R., Afolabi, O., & Omotoso, E. J. (2009). Delineation of saltwater intrusion into the freshwater aquifer of Lekki Peninsula, Lagos, Nigeria. *Environmental Geology, 56*(5), 927–933. doi:10.1007/s00254-008-1194-3. Available from: http://www.spingerlink.com/content/ekj1477561052r10/fulltext.pdf. Accessed 8 January 2009.

APHA (2005). *Standard methods for the examination of water and wastewater* (21st ed.). Washington DC: American Public Health Association. ISBN 0-87553-047-8.

Awni, T. B. (2006). Use of electrical resistivity methods for detecting subsurface fresh and saline water and delineating their interfacial configuration: a case study of the eastern Dead Sea coastal aquifers, Jordan. *Hydrogeology Journal, 14*, 1277–1283. doi:10.1007/s10040-006-0034-3. Available from: http://www.spingerlink.com/content/95613003427232r6/fulltext.pdf. Accessed 28 December 2008.

Baba, M. F. (1997). *Geology quaternary at Teluk Datuk area, state of Selangor (Sheet 101)*. Geology Quaternary Report, Department of Mineral and Geoscience Malaysia, Ministry of Natural Resources and Environment Malaysia. Malaysia Government.

Barker, R. & Moore, J. (1998). The application of time-lapse electrical tomography in groundwater studies. *The Leading Edge, 17*, 1454–1458. Available from: http://segdl.org/getpdf/servlet/GetPDFServlet?filetype=pdf&id=LEEDFF000017000014540000001&idtype=cvips. Accessed 13 April 2010.

Benkabbour, B., Toto, E. A. & Fakir, Y. (2004). Using DC resistivity method to characterize the geometry and the salinity of the Plioquaternary consolidated coastal aquifer of the Mamora plain, Morocco. *Environmental Geology, 45*(4), 518–526. doi:10.1007/s00254-003-0906-y. Available from: http://www.spingerlink.com/content/3ejfg3cn4t89r141/fulltext.pdf. Accessed 4 January 2009.

BS (British Standard) 1377 (1990). *Part 2: Method of test for soils for civil engineering purposes* (pp. 1–68). London: British Standard Institution. ISBN: 0580178676.

Cartwright, K., & McComas, M. R. (1968). Geophysical surveys in the vicinity of sanitary landfills in northeastern Illinois. *Ground Water, 5*, 23–30. Available from: http://info.ngwa.org/GWOL/pdf/682578001.PDF.

Cassiani, G., Bruno, V., Villa, A., Nicoletta Fusi, N., & Binley, A. M. (2006). A saline trace test monitored via time-lapse surface electrical resistivity tomography. *Journal of Applied Geophysics, 59*, 244–259. doi:10.1016/j.jappgeo.2005.10.007. Available from: http://www.sciencedirect.com/science?ob=MImg&_imagekey=B6VFC-4JOWRC5-1-8&_cdi=6007&_user=15079. Accessed 6 January 2010.

Dahlin, T., & Loke, M. H. (1998). Resolution of 2D Wenner resistivity imaging as assessed by numerical modelling. *Journal of Applied Geophysics, 38*(4), 237–249. PII:50926-9851(97)00030-X. Available from: http://www.sciencedirect.com/science?_ob=MImg&_imagekey=B6VFC-35x5299-8-1&-cdi=60078_user=15079. Accessed 8 January 2009.

Dey, A., & Morrison, H. F. (1979). Resistivity modelling for arbitrarily shaped two-dimensional structures. *Geophysical Prospecting, 27*(1), 106–136. doi:10.1111/j.1365-2478.1979.tb00961.x. Available from: http://www3.interscience.wiley.com/user/ID=119598599&Act=21388code=4726&Page=/cgi-bin/fulltext/11. Accessed 8 January 2009.

Di Sipio, E., Galgaro, A., & Zuppi, G. M. (2006). New geophysical knowledge of groundwater systems in Venice estuarine environment. *Estuarine, Coastal and Shelf Science, 66*, 6–12. doi:10.1016/j.ecss.2005.07.015. Available from: http://www.sciencedirect.com/science?_ob=MImg&_imagekey=B6WDV-4H6PKWO-1-H&cdi=67768_user=15079. Accessed 6 January 2010.

DSMM (2009). *Tide tables 2009 Malaysia* (pp. 52–72). Department of Survey and Mapping Malaysia.

DSMM (2010). *Tide tables 2010 Malaysia* (pp. 55–72). Department of Survey and Mapping Malaysia.

Ebraheem, A. M., Hamburger, M. W., Bayless, E. R., & Krothe, N. C. (1990). A study of acid mine drainage using earth resistivity measurements. *Ground Water, 28*(3), 361–368. Available from http://info.ngwa.org/GWOL/pdf/901550570.PDF. Accessed 6 January 2010.

Ebraheem, A. M., Senosy, M. M., & Dahab, K. A. (1997). Geoelectrical and hydrogeochemical studies for delineating groundwater contamination due to saltwater intrusion in the northern part of the Nile Delta, Egypt. *Ground Water, 35*(2), 216–222. Available from http://info.ngwa.org/GWOL/pdf/971262673.PDF. Accessed 6 January 2010.

Fetter, C. W. (2001). *Applied hydrogeology* (4th ed., p. 598). New Jersey: Prentice Hall. ISBN: 0131226878.

Golden Hope Plantation Berhad (2006). *Carey Island; a golden heritage; reliving history, preserving legacy, golden hope plantation Berhad* (pp 1–16). ISBN 967-969-547-6.

Hamzah, U., Yaacup, R., Samsudin, A. R., & Ayub, M. S. (2006). Electrical imaging of the groundwater aquifer at Banting, Selangor, Malaysia. *Environmental Geology, 49*(8), 1156–1162. doi:10.1007/s00254-005-0160-6. Available from: http://www.spingerlink.com/content/r8q5880065u3857/fulltext.pdf. Accessed 4 January 2009.

Ismail, R. (2008). *Construction and exploration of deep wells at Carey Island and Kg Kelanang, Kuala Langat District, Banting Selangor*. National Groundwater Resources Study under Subproject groundwater resources for State of Selangor. Report done by KS Global Sdn Bhd with collaboration Multical Card (M) Sdn Bhd under instruction the Department of Mineral and Geoscience Selangor State, Malaysia.

JICA MDGM (2002). *The study on the sustainable groundwater resources and environmental management for the Langat Basin in Malaysia* (Vol. 3). Japan International Cooperation Agency (JICA) and Mineral and Geoscience Department Malaysia (MDGM) Report.

Kemna, A., Vanderborght, J., Kulessa, B. & Harry Vereecken, H. (2002). Imaging and characterisation of

subsurface solute transport using electrical resistivity tomography (ERT) and equivalent transport models. *Journal of Hydrology, 3–4*(267), 125–146. Available from: http://www.sciencedirect.com/science?_ob=MImg&_imagekey=B6V6C-46NYFK8-2-44&-cdi=5811&_user=1507. PII: S0 02 2-1694 (02) 00145-2. Accessed 6 January 2010.

Loke, M. H., & Barker, R. D. (1996). Rapid least squares inversion of apparent resistivity pseudosection using a quasi-Newton method. *Geophysical Prospecting, 44*(3), 131–152. GPPRAR44(1)1-178(1996). ISSN 0016-8025.

Loke, M. H., Acworth, I., & Dahlin, T. (2003). A comparison of smooth and blocky inversion methods in 2D electrical imaging surveys. *Exploration Geophysics, 34*(3), 182–187. (Available online at www.geoelectrical.com/downloads.php and email to mhloke@tm.net.my).

Loke, M. H. (1999). Time lapse resistivity imaging inversion. In *Proceedings of the 5th meeting of the EEGS European section, Em1*. Available online at www.geoelectrical.com/timeabs.pdf.

Loke, M. H. (2010a). *Tutorial: 2-D and 3-D electrical imaging surveys* (pp. 1–145). Available online at www.geoelectrical.com/downloads.php.

Loke, M. H. (2010b). *RES2DINV ver. 3.59 for Windows XP/Vista/7 for rapid 2-D resistivity and IP inversion using the least squares method* (pp 1–148). Available online at www.geoelectrical.com/downloads.php.

Maillet, G. M., Rizzo, E., Revil, A., & Vella, C. (2005). High resolution electrical resistivity tomography (ERT) in a transition zone environment: application for detailed internal architecture and infilling processes study of a Rhone River paleo-channel. *Marine Geophysical Researches, 26*, 317–328. doi:10.1007/s11001-005-3726-5. Available from: http://www.spingerlink.com/content1y1x7m7247q5x40p6/fulltext.pdf. Accessed 6 January 2010.

Ngah, D. S. (1988). *Groundwater investigation for determination of suitability using hand-pump at rural area of Kuala Langat District, Selangor Darul Ehsan, Report No. GPH1/1988*. Department of Mineral and Geosciences Malaysia, Ministry of Natural Resources and Environment.

Ogilvy, R. D., Meldrum, P. I., Kuras, O., Wilkinson, P. B., Chambers, J. E., Sen, M., et al. (2009). Automated monitoring of coastal aquifers with electrical resistivity tomography. *Near Surface Geophysics, 7*(5–6), 367–375. doi:10.3997/1873-0604.2009027. (Available online at http://nora.nerc.ac.uk/8645/).

Oldenborger, G. A., Knoll, M. D., Routh, P. S., & LaBrecque, D. J. (2007). Time-lapse ERT monitoring of an injection/withdrawal experiment in a shallow unconfined aquifer. *Geophysics, 72*, 177–188. doi:10.1190/1.2734365. http://www.eos.ubc.ca/~goldenbo/geop0313.pdf. Accessed 6 January 2010.

Olofsson, B., & Lundmark, A. (2009). Monitoring the impact of de-icing salt on roadside soils with time-lapse resistivity measurements. *Environmental Geology, 57*, 217–229. doi:10.1007/s00254-008-1302-4. Available from: http://www.spingerlink.com/content/j00744004jqn8062/fulltext.pdf. Accessed 6 January 2010.

Pujari, P. R., & Soni, A. K. (2008). Sea water intrusion studies near Kovaya limestone mine, Saurashtra coast, India. *Environmental Monitoring Assessment, 154*(1–4), 93–109. doi:10.1007/s10661-008-0380-9. Available from: http://www.spingerlink.com/content/5w365533728128x2/fulltext.pdf. Accessed 6 January 2010.

Samsudin, A. R., Haryono, A., Hamzah, U., & Rafek, A. G. (2008). Salinity mapping of coastal groundwater aquifers using hydrogeochemical and geophysical methods: A case study from north Kelantan, Malaysia. *Environmental Geology, 55*(8), 1737–1743. doi:10.1007/s00254-007-1124-9. Available from: http://www.spingerlink.com/content/6865279tg71287u5/fulltext.pdf. Accessed 3 January 2009.

Sherif, M., El Mahmoudi, A., Garamoon, H., Kacimov, A., Akram, S., Ebraheem, A., et al. (2006). Geoelectrical and hydrogeochemical studies for delineating seawater intrusion in the Outlet of Wadi Ham, UAE. *Environmental Geology, 49*(4), 536–551. doi:10.1007/s00254-005-0081-4. Available from: http://www.spingerlink.com/content/7w07144t21663226/fulltext.pdf. Accessed 4 January 2009.

Suntharalingam, T., & Teoh, L. H. (1985). *Quaternary geology of the coastal plains of Taiping*. Quaternary Geology Report. Geological Survey Malaysia. Ministry of Primary Industries Malaysia.

Suratman, S., & Awang, N. (1998). *Recent groundwater studies in the Klang Valley, Selangor Malaysia* (Vol. 24, p. 315). Warta Geologi Geological Society of Malaysia.

Tahir, H., & Abdul Hamid, I. (2003). *The study of groundwater resource at Teluk Gong, Pelabuhan Kelang, Selangor Darul Ehsan*. Report No. JMG.SWP (HG) 03/2003. Department of Mineral and Geosciences Malaysia, Ministry of Natural Resources and Environment.

Wilson, S. R., Ingham, M., & McConchie, J. A. (2006). The applicability of earth resistivity methods for saline interface definition. *Journal of Hydrology, 316*, 301–312. doi:10.1016lj.jhydrol.2005.05.004. http://www.sciencedirect.com/science?-ob=MImg&_imagekey=B6V6C-4GFCR6N-4-R&_cdi=5811&_user=15079. Accessed 6 January 2010.